Airway mechanics, gas exchange, and blood flow in a nonlinear model of the normal human lung

C. H. LIU,[1] S. C. NIRANJAN,[2,3,4] J. W. CLARK, JR.,[2,3]
K. Y. SAN,[1] J. B. ZWISCHENBERGER,[2,5] AND A. BIDANI[2,4]
(With the Technical Assistance of H. B. Winnike, C. Vanouye, and J. B. Olansen)
Departments of [1]Chemical Engineering and [3]Electrical and Computer Engineering, Rice University, Houston, 77251; and [2]Biomedical Engineering Center, Departments of [4]Internal Medicine and [5]Thoracic Surgery, University of Texas Medical Branch, Galveston, Texas 77555

Liu, C. H., S. C. Niranjan, J. W. Clark, Jr., K. Y. San, J. B. Zwischenberger, and A. Bidani. Airway mechanics, gas exchange, and blood flow in a nonlinear model of the normal human lung. *J. Appl. Physiol.* 84(4): 1447–1469, 1998.—A model integrating airway/lung mechanics, pulmonary blood flow, and gas exchange for a normal human subject executing the forced vital capacity (FVC) maneuver is presented. It requires as input the intrapleural pressure measured during the maneuver. Selected model-generated output variables are compared against measured data (flow at the mouth, change in lung volume, and expired O_2 and CO_2 concentrations at the mouth). A nonlinear parameter-estimation algorithm is employed to vary selected sensitive model parameters to obtain reasonable least squares fits to the data. This study indicates that *1*) all three components of the respiratory model are necessary to characterize the FVC maneuver; *2*) changes in pulmonary blood flow rate are associated with changes in alveolar and intrapleural pressures and affect gas exchange and the time course of expired gas concentrations; and *3*) a collapsible midairway segment must be included to match airflow during a forced expiration. Model simulations suggest that the resistances to airflow offered by the collapsible segment and the small airways are significant throughout forced expiration; their combined effect is needed to adequately match the inspiratory and expiratory flow-volume loops. Despite the limitations of this lumped single-compartment model, a remarkable agreement with airflow and expired gas concentration measurements is obtained for normal subjects. Furthermore, the model provides insight into the important dynamic interactions between ventilation and perfusion during the FVC maneuver.

ventilation; perfusion; convective-diffusion transfer; parameter estimation; pulmonary function testing

HUMAN EXTERNAL RESPIRATION is a complex process consisting of at least three component parts: *1*) ventilation via airways and lung mechanics; *2*) perfusion of lung via the pulmonary circulation; and *3*) gas exchange based on the transport of species across the alveolar-capillary barrier and the O_2-CO_2 binding properties of blood. Mathematical modeling to date has focused largely on the component parts, i.e., either exclusively on airway mechanics (14, 23, 25, 54), lung mechanics (18, 49, 50–52), gas exchange (22, 27, 34, 35), pulmonary circulation (8, 9, 26), occasionally on the linkage of any two components (17, 29, 43, 46, 56), but never on a treatment involving all elements collectively. This study attempts to describe the three constituent components concurrently, including the inherent coupling between them.

In an effort to characterize the dynamics of the forced vital capacity (FVC) maneuver in normal human subjects, a nonlinear one-compartment mathematical model of respiration combining airway/lung mechanics, pulmonary blood flow, and gas exchange is presented. Measured intrapleural pressure waveforms generated during the execution of the FVC maneuver were used as model input. The FVC maneuver was chosen as the appropriate driving function, since it involves the generation of full muscular effort covering the full range of admissible lung volumes. A nominal set of model parameter values is derived by using information from a variety of sources, including *1*) our previous studies of airway mechanics (20, 40), *2*) the pulmonary circulation report of Milnor (37), and *3*) the pulmonary gas-transport model of Flummerfelt and Crandall (17). A nonlinear least squares estimation algorithm (Marquardt) was employed to adjust a sensitive subset of model parameters to achieve an acceptable fit to measured data. The ventilation and perfusion models are naturally coupled within the gas-transport model. Additional interactions between intrapleural and alveolar pressures and pulmonary blood volume occur during the FVC maneuver. Specifically, this affects the time course of the observed expired gas (O_2 and CO_2) concentration (see RESULTS).

This study aims to *1*) describe a methodology for characterizing data collected during the performance of the FVC maneuver, and *2*) provide biophysically based explanations of the interactions between ventilation and perfusion and the concomitant effects on gas exchange. A theoretical basis for physiological interpretation of events occurring during the execution of an FVC maneuver is provided. A subset of output variables predicted by the model and compared against data includes changes in lung volume, airflow at the mouth, and the partial pressures of O_2 and CO_2 in the expired gas. The model also yields predictions of quantities not

measured routinely, such as *1*) alveolar pressure, *2*) excursions in airway resistance and lung compliance, *3*) gas composition in the airways, *4*) blood perfusion rates, and *5*) capillary blood volume variation. Direct measurement of these latter quantities cannot be obtained clinically without invasive procedures. The crucial role of component dynamics during the FVC maneuver is analyzed and discussed. Model-based sensitivity analysis reveals that parameters associated with all three of the forenamed respiratory components affect and influence the data. Feasibility and predictive capability are established by characterizing the data collected from four normal subjects.

METHODS

Model Development

The choice of the specific model structure adopted was motivated by the requirements that the model *1*) satisfactorily describe the dynamics of airway/lung mechanics over the full range of lung volumes from residual volume (RV) to total lung capacity (TLC) (therefore, a nonlinear description); *2*) emulate flow-limiting behavior during forced expiration (hence, use of a resistive-compliant collapsible midairway segment); *3*) simulate temporal profiles of expired gas concentration in normal subjects during the FVC maneuver; and *4*) describe changes in gas exchange and perfusion rates. A schematic diagram of the complete model incorporating airway mechanics, gas exchange, and pulmonary circulation is depicted in Fig. 1*A*, along with an equivalent representation of the corresponding pneumatic and hydraulic subsystems in Fig. 1, *B* and *C*, respectively. The readers are referred to APPENDIX A for a complete description of the dynamic equations comprising the model.

Glossary

C_A	Compliance of alveolar compartment, l/cmH_2O
$Caw_i^{(k)}$	Concentration of species *i* in the k^{th} airway compartment, gram-mol/l
C_{clp}	Compliance of collapsible airway segment, l/cmH_2O
Cpc	Compliance of lumped pulmonary capillary region, l/mmHg
$Cb_i^{(j)}$	Total content of gaseous species *i* in blood in compartment *j*, ml *i*/ml blood
$\overline{C}$pc	Mean pulmonary capillary compliance during passive breathing, l/mmHg
D_{L_i}	Lung diffusing capacity of species *i*, ml [STPD]$\cdot min^{-1}\cdot mmHg^{-1}$
K_1	Linear resistance of upper airways, cm$H_2O\cdot l^{-1}\cdot s$
K_2	Flow-dependent resistance of upper airways, cm$H_2O\cdot l^{-2}\cdot s^2$
K_3	Magnitude of R_C at $V_C = V_{C_{max}}$, cm$H_2O\cdot l^{-1}\cdot s$
L_{pc}	Length of pulmonary capillary, cm
N_{seg}	Discretized number of segments in the capillary, 35
N_{tot}	Total number of gaseous species considered in this study, 3
P_{A_i}	Partial pressure of species *i* in the alveolar space, Torr
P_{C_i}	Partial pressure of species *i* in the collapsible airway, Torr
P_{D_i}	Partial pressure of species *i* in the upper airway (dead space), Torr
Pam_i^{sat}	Saturated partial pressure of species *i* in the ambient, Torr
P_A	Total pressure in alveolar region, cmH_2O
P_C	Total pressure in collapsible region, cmH_2O
P_D	Total pressure in rigid dead space region, cmH_2O
P_E	Total pressure in the external ambient, cmH_2O
Pel	Lung elastic recoil, cmH_2O
Pel^E	Outer envelope of Pel during expiratory phase, cmH_2O
Pel^I	Outer envelope of Pel during inspiratory phase, cmH_2O
Pel_{max}	Pel at $V_A = V^*$, cmH_2O
P_{H_2O}	Partial pressure of water vapor, Torr
Ppl	Intrapleural pressure, cmH_2O
Ppl_{mean}	Equilibrium intrapleural pressure during tidal breathing, cmH_2O
Ppl_{min}	Minimum intrapleural pressure achieved during FVC maneuver, cmH_2O
Ppl_{max}	Maximum intrapleural pressure achieved during FVC maneuver, cmH_2O
P_ϕ	Constant characterizing arterial and venous resistance relation to effort (typically, greater than $-Ppl_{min}$), cmH_2O
$\overline{Ppl}$	Spatially averaged intrapleural pressure relative to reference, cmH_2O
P_S	Standard pressure, 760 mmHg
Ptm	Transmural pressure across collapsible airway, cmH_2O
Ptm_b	Transmural pressure across pulmonary capillary, cmH_2O
Ptm_{max}	Ptm at $V_C = V_{C_{max}}$, cmH_2O
Pa	Total pressure in pulmonary artery (and arterioles), Torr
$Pb_i^{(j)}$	Partial pressure of species *i* in blood in segment *j*, Torr
Ppc	Total pressure in pulmonary capillary, Torr
Pv	Total pressure in pulmonary veins (and venules), Torr
Ppa	Transmural pulmonary arterial pressure relative to $\overline{Ppl}$, Torr
Ppv	Transmural pulmonary venous pressure relative to $\overline{Ppl}$, Torr
P_{ref}	Reference pressure at T_{body}, Torr
$P_{E_{O_2}}$	Partial pressure of O_2 in expired gas at mouth, Torr
$P_{E_{CO_2}}$	Partial pressure of CO_2 in expired gas at mouth, Torr
$\dot{Q}_{CA}$	Airflow rate between the collapsible airway and alveolar space, l/s
$\dot{Q}_{DC}$	Airflow rate between the dead space and collapsible airways, l/s
$\dot{Q}_{ED}$	Airflow rate in the upper airways, l/s
$\dot{Q}_b^{in}$	Blood flow rate into pulmonary capillary, l/s
$\dot{Q}_b^{out}$	Blood flow rate out of pulmonary capillary, l/s
R_C	Collapsible airway resistance, cm$H_2O\cdot l^{-1}\cdot s$
R_L, ti	Pulmonary tissue resistance, cm$H_2O\cdot l^{-1}\cdot s$
Rs	Small airway resistance, cm$H_2O\cdot l^{-1}\cdot s$
Rs_a	Parameter characterizing curvature of Rs
Rs_c	Rs at V^*, cm$H_2O\cdot l^{-1}\cdot s$
$Rs_{c\,max}$	Rs_c at the instant of $Ppl = Ppl_{max}$ (>0), cm$H_2O\cdot l^{-1}\cdot s$
Rs_m	Magnitude of $(Rs - Rs_c)$ at minimal alveolar volume, cm$H_2O\cdot l^{-1}\cdot s$
Ruaw	Upper airway resistance, cm$H_2O\cdot l^{-1}\cdot s$
Ra	Pulmonary arterial (and arteriolar) resistance, mmHg$\cdot l^{-1}\cdot s$
Ra_0	Approximately mean Ra during passive breathing, mmHg$\cdot l^{-1}\cdot s$
Rpc	Pulmonary capillary resistance, mmHg$\cdot l^{-1}\cdot s$

Rpc_0	Magnitude of Rpc at Vpc = Vpc_{max}, mmHg·l^{-1}·s
Rv	Pulmonary venous (and venuolar) resistance, mmHg·l^{-1}·s
Rv_0	Approximately mean Rv during passive breathing, mmHg·l^{-1}·s
T_{body}	Body temperature, 310 K
T_{am}	Ambient temperature, 298 K
T_S	Standard temperature, 273 K
V*	Alveolar volume at end inspiration, assuming that $\overline{Ppl} = Ppl_{min}$ at all times during forced inspiration, liters
$\dot{V}_{A_o}$	Airflow rate at the mouth detected by pneumotachometry, l/s
VA	Alveolar volume, liters
Vpc	Pulmonary capillary volume, liters
Vpc_{max}	Maximum pulmonary capillary volume, liters
VC	Collapsible airway volume, liters
VC_{max}	Maximum collapsible airway volume, liters
VD	Anatomic dead space volume, liters
VL	Total lung volume (=VA + VC + VD), liters
V_{crit}	Lung volume at which Rs increases abruptly during forced expiration, liters
V_ϕ	Parameter characterizing volume dependence of Ra and Rv, cmH_2O·l^{-5}·s
$V_{z_b}^{(j)}$	Mean molar-averaged axial velocity of blood flow in capillary segment *j*, l/s
ϕ_i	Rate of transfer of species *i* between blood and alveolar region, ml (STPD) *i*/min
Φ_{tot}^*	Total rate of transfer of all species, ml (STPD)/min
ρ_A	Overall density of air in alveolar region, g/l
ρ_C	Overall density of air in collapsible airway region, g/l
ρ_D	Overall density of air in dead space region, g/l
ρ_{ref}	Overall density of air in ambient under reference conditions, g/l
ξ	Scale factor used to create inspiratory Pel for each subject

Airway/lung mechanics model. The general form is similar to that previously reported (20, 40). A brief review of the model with incorporated modifications is provided below.

THORACIC CAGE AND RESPIRATORY MUSCLES. The lung and airways were assumed to be enclosed within a rigid-walled thoracic cage, with the airways open to the atmosphere. The intrapleural space was assumed to be subject to a time-varying, spatially averaged driving intrapleural pressure [$\overline{Ppl}(t)$], which was assumed to be equivalent to the average pressure in the pleural space acting on the lungs and produced by the muscles of respiration. Excursion in $\overline{Ppl}$ was dictated by the effort generated by the subject.

ALVEOLAR REGION. Alveolar region (of volume VA) was assumed to exhibit nonlinear, time-varying viscoelastic behavior (18, 24, 51, 52). Static elastic behavior of the lung (Pel vs. VA) was described by a hysteretic pressure-volume (P-V) relationship (see APPENDIX A for details). The extent of hysteresis in Pel was presumed to be a function of breathing effort, which, in turn, was assumed to be proportional to $\overline{Ppl}$ (reflecting muscular effort). Hence, the dependence of Pel on $\overline{Ppl}$ served to define the well-known hysteretic path (31). Viscous dissipative characteristics exhibited by lung tissue (1, 18) were characterized by using a constant lung tissue resistance (RL, ti).

PERIPHERAL AIRWAYS. Peripheral airways were characterized by a resistance (Rs) that was inversely proportional to VA (20, 40). Airway closure during forced expiration causes occlusion of these airways at low alveolar volumes (4, 6, 13, 39, 42). Because of the effect of large intrathoracic pressures generated during the effort-dependent portion of forced expiration, Rs was modified to be a function of both VA and $\overline{Ppl}$.

COLLAPSIBLE AIRWAY REGION. Collapsible airway region (of volume VC) has been characterized before in terms of a volume-dependent resistance and a volume-pressure relationship (VC-Ptm) (20, 40). The functional importance of this collapsible segment has since been confirmed by Barbini et al. (2), who analyzed the input impedance spectrum vs. frequency and demonstrated that adequate reconstruction of pressure-flow data could not be achieved with a conventional single-compartment resistive-compliant model. Previous studies have demonstrated that in lumped models expiratory flow limitation during the FVC maneuver cannot be simulated without the presence of this collapsible segment (2, 40). Verbraak et al. (55) modeled the elastic properties of the compressible segment as a family of curves dependent on the lung elastic recoil. This more complex approach proved to be of little benefit in achieving good fits to subject data, and, hence, the original formulation was utilized in this work.

UPPER AIRWAY REGION. Upper airway region (of volume VD) was assumed to be rigid, with its resistance to airflow characterized by a nonlinear, flow-dependent Rohrer resistor (23), as in Refs. 20 and 40.

Pulmonary circulation model. The pulmonary capillaries were considered as a single tubular compartment of constant length of 0.05 cm (17) and a variable volume. The lumped pulmonary circulation model developed (Fig. 1*C*) was based on the following assumptions. *1*) Upstream pulmonary arterial pressure (Ppa) and downstream pulmonary venous pressure (Ppv) were assumed to be constant at 15 and 5 Torr, respectively, referenced to intrapleural pressure (26, 58). *2*) Pulmonary vascular resistance was partitioned into three components: a proximal, precapillary arteriolar resistance (Ra); a pulmonary capillary resistance (Rpc); and a distal, postcapillary venous resistance (Rv). Perivascular pressure was assumed to be intrapleural pressure for the proximal and distal (extra-alveolar vessels) but alveolar pressure for the capillary (intra-alveolar vessel). The proximal and distal resistances were assumed to be inversely proportional to VA but proportional to the pleural pressure (15, 21), whereas the capillary resistance was presumed to be affected solely by alveolar pressure (37). Blood flow rate into and out of the capillary ($\dot{Q}_b^{in}$ and $\dot{Q}_b^{out}$, respectively) was then governed by the nodal pressure drops (Pa, Ppc and Pv) developed across the corresponding vascular resistances. Consequently, capillary blood volume (Vpc) was modulated by the inequality between blood inflow and outflow and the transmural pressure across the lumped capillary wall.

Gas exchange model. Gas exchange occurring in the constant-volume dead space and variable-volume collapsible and alveolar compartments was described by using species-conservation laws. On the air side of the exchanger, it was assumed that inspired air was instantaneously warmed to body temperature and fully saturated with water vapor. The gaseous mixture was presumed to obey the ideal gas law. On the blood side, the discrete constituents (plasma and erythrocytes) were lumped together and assumed to statistically behave as a uniform, homogeneous phase (3). Within a control volume, the instantaneous specific reactions were then considered to be at equilibrium; relationship between species content and their corresponding equilibrium partial pressures was consequently represented by empirical dissociation curves (12, 28, 48). One-dimensional axial convection provided the sole means for bulk transport of blood and movement of species along the pulmonary circulation; diffusion in the radial and axial directions was ignored. Two-phase flow created due to blood heterogeneity was further disregarded.

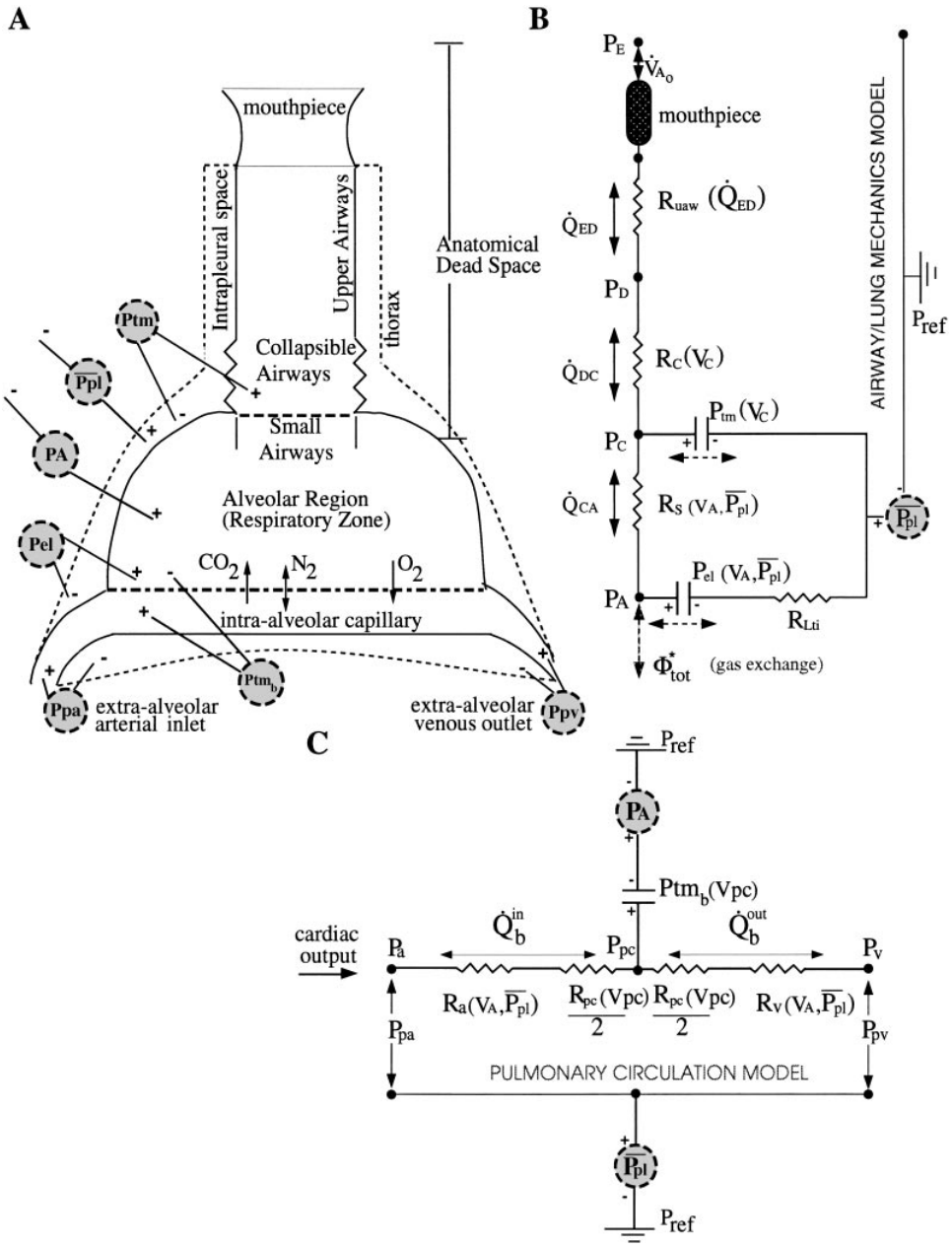

Fig. 1. Schematic representation of airway/lung mechanics, gas exchange, and pulmonary circulation system. Symbols are explained in *Glossary*. *A*: components of airway mechanics, pulmonary circulation, and gas exchange model. *B*: pneumatic representation of airway/lung mechanics and gas exchange. *C*: hydraulic representation of pulmonary circulation.

Transport of gaseous species across the alveolar-capillary membrane, assumed to be solely by diffusion, was characterized by a lumped species lung diffusing capacity (D_{L_i}), which accounted for the total diffusion-resistive path taken by species i ($i = O_2$, CO_2, N_2) as it diffused across the alveolar-capillary barrier. O_2 was taken up by the blood, and CO_2 was excreted, whereas N_2 (a relatively inert gas) diffused in either direction, depending on the instantaneous overall ventilation-perfusion ratio (39). The contribution of the physiological shunt (35) was neglected. The model used here was directly adapted from Flummerfelt and Crandall (17), with the provision that alveolar pressure was not held atmospheric but, rather, was calculated via the airway mechanics model.

Experimental Pulmonary Measurements

Measurements of airflow at the mouth, expired P_{CO_2} and P_{O_2} at the mouth, and esophageal pressure were made in four volunteer human male subjects in the Pulmonary Function Laboratory at John Sealy Hospital, Galveston, TX. A System 2800 Autobox Body Plethysmograph with associated pneumotachometer from SensorMedics (Dayton, OH) was used to perform the tests as well as to collect the data. A latex balloon was inserted through the subject's nose and positioned in the esophagus (nasogastric), at a location where the largest pressure deflection could be observed. The balloon was then connected to a pressure transducer in the body box. Expired gas was sampled continuously at the mouthpiece and analyzed by a Datex Capnomac Ultima System to yield continuous measurements of CO_2 and O_2 concentrations in the expirate. The CO_2 and O_2 data exhibited time delay; their traces were manually synchronized to the recordings of the pressure and flow data to accommodate the resulting transportation lag. The esophageal pressure signal [assumed equivalent to intrapleural pressure (36)] was sampled at 50 Hz (i.e., sampling interval = 0.02 s), which was more than adequate to ensure the reproduction of the pressure signal from its

samples (the maximum Nyquist sampling rate was calculated to be 40 Hz, based on the Fourier transforms of the flow data that had the highest frequency content of all the recorded waveforms). The functional residual capacity (FRC) was obtained by having the subject pant against a closed shutter. Analog recordings were digitally sampled by using a National Instruments NB_MIO-16x DAQ board and an AMUX-64T multiplexer board, controlled by using LabVIEW 4.0 software, all of which were connected to a Macintosh Quadra 800. LabVIEW virtual instruments were developed to *1*) acquire continuous waveform data from multiple analog channels; *2*) integrate airflow data to obtain instantaneous thoracic gas volume data; *3*) continually display flow-volume plots; *4*) calibrate (direct or volume referenced) input transducers; *5*) apply a Butterworth filter to lightly smooth the data; and *6*) accummulate data records in separate ASCII files as needed. For the FVC maneuver, the subject deflated the lung to close to RV and, without pausing, inflated fully to TLC. Again without pausing, the subject exhaled forcefully to RV until no airflow was detected at the mouth. The maneuver was completed with another forceful inspiration to TLC.

Each experimental episode was recorded after the subject rested adequately (for ~5 min) and followed by several cycles of tidal breathing to ensure full recovery. The end-tidal gas composition was monitored to ensure that the CO_2 level reached 39–40 Torr. When this level was achieved, it was assumed that a steady-state condition had been reached and that the mixed venous blood tension achieved constant nominal values consistent with those commonly reported (59). The duration of the recording episode was <1 min; hence, it was presumed that the mixed venous composition did not change significantly during this time. This seemingly reasonable modeling assumption does require experimental verification, however. Within the noninvasive constraints observed in the pulmonary function laboratory (except for the use of a nasogastric esophageal balloon), it is unlikely that such a measurement could be adopted easily. Four volunteer human subjects with normal lung function (i.e., no respiratory abnormalities) were recruited for this study. Their particulars are listed in Table 1.

Computational Aspects

A block diagram depicting the overall implementation is shown in Fig. 2. Measured $\overline{Ppl}$ associated with the FVC maneuver [first filtered by using a zero-phase shift, third-order Butterworth digital filter (41) to reduce cardiogenic artifacts] was used as the input to the model. Other information necessary to initialize the model included *1*) analytic descriptions of P-V relationships associated with the collapsible airway segment, alveolar region, and the lumped pulmonary capillary; *2*) the pressure-flow relationships that characterize resistances of the upper, collapsible, and small airways; pulmonary arterial; and capillary and venous resistances; *3*) gas composition of inspired air; and *4*) mixed venous blood-gas composition (assumed constant for reason explained in *Experimental Pulmonary Measurements*). Model implementation of the ensuing system of ordinary differential equations was done in the C programming language. Numerical integration of the differential equations was performed by using Epsode (5), with a tolerance of 10^{-4} s and a maximum time step size of 5×10^{-3} s. A subset of model output (lung volume variation, flow at the mouth, and expired gas concentration) was compared against the data obtained in the pulmonary function laboratory. A parameter-estimation algorithm was applied to adjust a selected set of sensitive parameters so as to achieve acceptable fits to data for a particular normal subject during the FVC maneuver.

Table 1. *Physical parameters for volunteer subjects*

Subject No.	Age, yr	Height, in.	Weight, lb.	BSA, m^2	FRC, liters*	RV, liters*	TLC, liters*
1	34	70	185	2.02	2.42	1.24	5.19
2	39	72	165	1.96	4.54	2.04	8.27
3	38	66	161	1.82	3.04	1.61	6.34
4	40	72	180	2.04	2.78	1.91	7.20

FRC, functional residual capacity; RV, residual volume; TLC, total lung capacity. Calculation for body surface area (BSA) was based on formula from Ref. 7: BSA (m^2) = weight (lb.)$^{0.425}$ × height (in.)$^{0.725}$ × 1.009×10^{-2}. *Determined from calculations implemented in body plethysmograph.

Parameter Estimation

Values for the adjustable parameters were obtained by using an iterative nonlinear least-squares parameter-identification method, viz., Marquardt (30). A sequential process was adopted for parameter estimation. In the first stage, only flow at the mouth and lung volume were used as data to estimate parameters describing airway mechanics. The estimation was performed separately for the inspiratory and expiratory phases by using subsets of parameters in each phase. In the second stage, O_2 and CO_2 concentrations at the mouth were used as data to obtain estimates on parameters related to gas exchange and pulmonary circulation. During this time, the parameter estimates obtained from the first stage were held constant. This adjustment strategy was justified based on the observation that changes in pulmonary circulation model parameters did not affect the results achieved in tuning the airway/lung mechanics model. Further details on this aspect are furnished in APPENDIX B.

For practical reasons, it was necessary to have good nominal values for parameters to ensure convergence of the estimation algorithm. Initial simulations employing parameter values from previous studies (see introductory section) provided initial fits. Further manual adjustment yielded even better fits to the data, ultimately leading to a nominal set of model parameters that was used to initialize the Marquardt scheme (30). The adjustable parameters were chosen based on their known influence on portions of the maximum flow-volume curve associated with the FVC maneuver, as well as parameter variation checks performed in a separate study (not presented here), by using relative sensitivity coefficients to assess the sensitivity of flow and volume to these variations. The estimation algorithm was terminated when the maximum relative change in the adjustable parameters did not exceed 1% on subsequent iterative cycles.

RESULTS

Model predictions compared against data for a human subject performing an FVC maneuver are shown in Fig. 3. The last cycle of tidal breathing before the subject exhaled to RV prior to the onset of the FVC maneuver is also shown for reference. Note that the major features of the loop predicted by the model (depicted by solid lines in Fig. 3), such as peak inspiratory flow, initial expiratory upstroke slope, peak expiratory flow, and final expiratory slope, all agree reasonably well with the experimental data.

Airway Mechanics

A phase-plane plot called the "maximal flow-volume" loop is constructed in Fig. 3*A*. The dynamic description

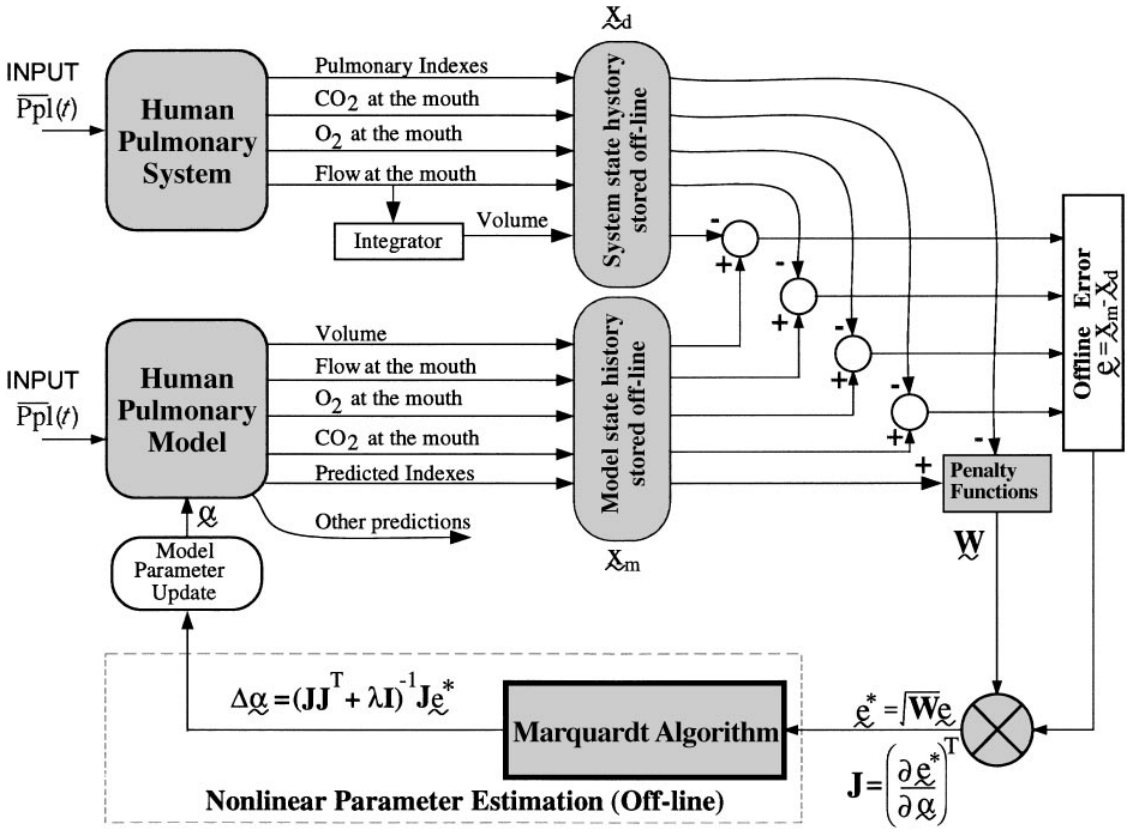

Fig. 2. Block diagram of simulation implementation. Intrapleural pressure is input to both the actual system and the mathematical model. Measured output variables are compared off-line against corresponding prediction. A nonlinear least square parameter-estimation algorithm is utilized to modify and estimate model parameter values to minimize discrepancy between measurements and the corresponding model predictions during forced vital capacity (FVC) maneuver. λ denotes the Levenburg adjustment parameter. See *Glossary* for other definitions.

is restricted solely to the FVC portion of the maneuver. During the early inspiratory phase, $\overline{Ppl}(t)$ drops considerably lower than baseline values (Fig. 3*B*) and is transmitted across the alveolar wall creating subatmospheric alveolar pressure (P_A), as indicated in Fig. 3*C*. The ensuing elevation in transairway pressure gradient ($P_E - P_A$) favors airflow into the lungs (Fig. 3*D*), causing their subsequent inflation (Fig. 3*E*). As inspiration proceeds, however, P_A reverts to equilibrium because of continued air filling (Fig. 3*C*), thereby lowering the transairway pressure gradient and leading to a reduction in the flow at the mouth (Fig. 3*D*). During the early portion of the forced expiration, both $\overline{Ppl}$ and P_A rise sharply to positive levels much greater than the normal baseline values (Fig. 3, *B* and *C*). The reversal in direction and elevated magnitude of the transairway pressure gradient now causes maximal or peak expiratory airflow at the mouth (Fig. 3*D*), resulting in a rapid drop in lung volume from TLC (Fig. 3*E*). As expiratory effort continues, $\overline{Ppl}$ and P_A remain positive, and V_{A_o} gradually approaches zero while lung volume declines to RV (Fig. 3, *D* and *E*). The model was constrained to limit lung volumes to never fall below RV. The corresponding excursion in the volume of the collapsible segment V_C during FVC is shown in Fig. 3*F*. It rises steeply during the inspiratory phase and falls rapidly to very low values as it experiences the full effect of positive transmural pressure during the prolonged forced expiratory period. At low alveolar volumes, high Rs causes the collapsible volume to inflate rapidly. Subsequent increase in V_A increases peripheral airway patency, thereby lowering Rs. This facilitates outflow from the collapsible segment into the alveolar region, causing the momentary dip in V_C (Fig. 3*F*) just after the onset of inspiration. This is termed as "serial pendelluft."

Pulmonary Circulation

Nodal driving pressure drops (Pa − Ppc and Ppc − Pv) and the corresponding transnodal resistances dictate blood flow rates and capillary blood volume changes. The dynamics of circulation are easily explained by considering nodal pressures referenced to intrapleural pressure, namely, Ppc referenced to intrapleural pressure, i.e., $Ppc' \equiv Ppc - \overline{Ppl}$ ($= Ptm_b + Pel + R_L, ti\, V_{A_o}$), whereas the new arterial and venous pressures referenced to intrapleural pressure (designated by Ppa and Ppv, respectively, and depicted as dotted lines in Fig. 4*A*) are arbitrarily set at 15 and 5 Torr, respectively, for these calculations. Figure 4*A* depicts these modified nodal pressures referenced to $\overline{Ppl}$ as well as the transmural pressure across the capillary wall, Ptm_b. As the subject inspires from RV (i.e., i → e*), reduction in Ra

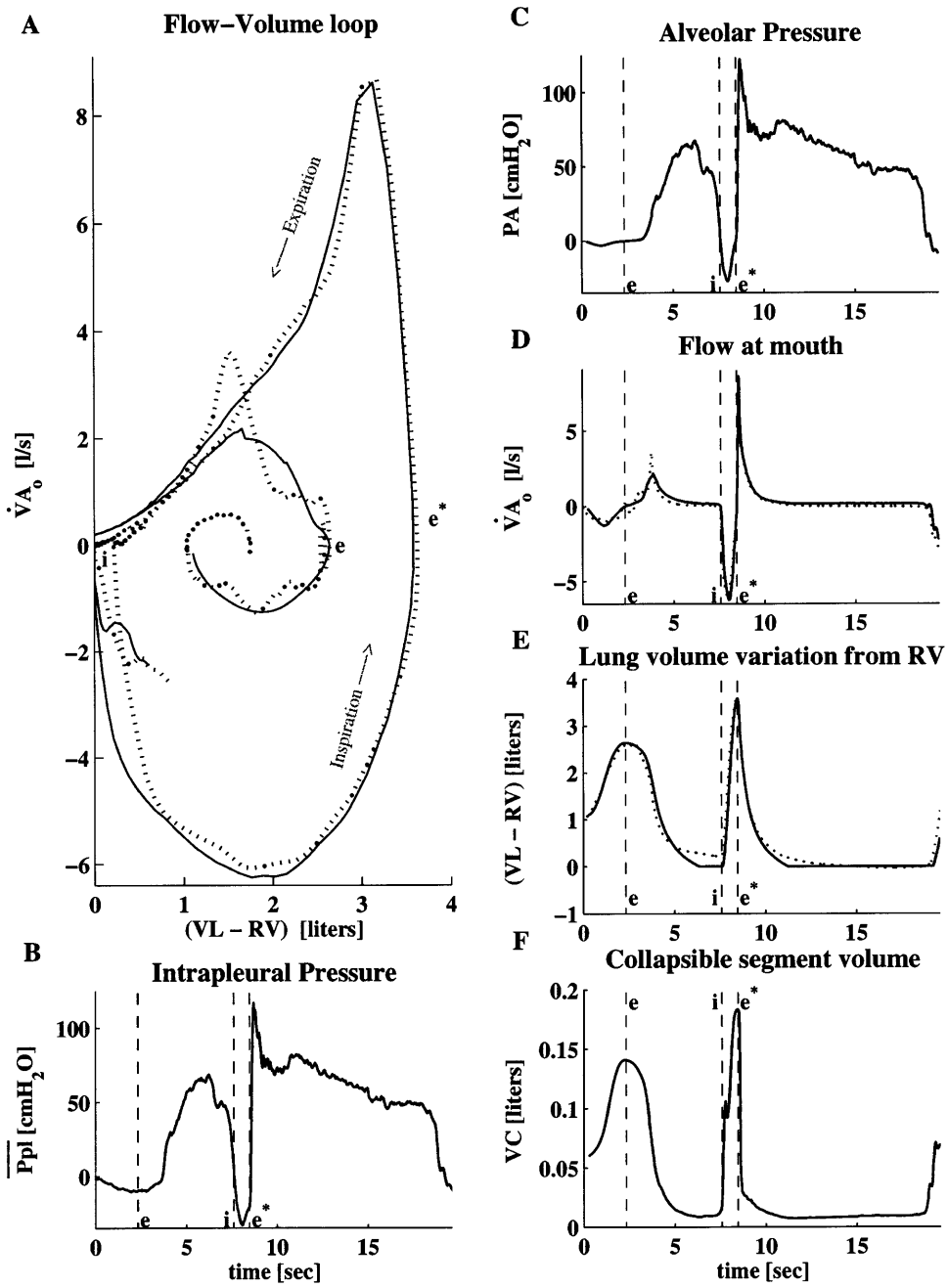

Fig. 3. Vital capacity maneuver. Model predictions are denoted by solid lines, and the measured data are represented as dots. In *B–F*, vertical dashed lines (from *left* to *right*, marked as *e*, *i*, *e**, respectively) mark the transition to residual volume (RV), inspiration from RV to total lung capacity (TLC) with full effort, and forced expiration from TLC to RV during FVC. *A*: plot of maximal flow-volume loop for a subject. *B*: intrapleural pressure generated by the subject during FVC maneuver. *C*: alveolar pressure developed. *D*: flow at mouth. *E*: lung volume variation from RV. *F*: collapsible segment volume. See *Glossary* for other definitions.

and Rv due to alveolar inflation (thin lines, Fig. 4*B*) creates an increase in both inlet and outlet blood flow rates at the capillary (Fig. 4*C*). The difference in inlet and outlet blood flow rates ($\dot{Q}_b^{in}$ and $\dot{Q}_b^{out}$, respectively), caused by the disparity in (Ppa − Ppc′) and (Ppc′ − Ppv), respectively, results in a slight decrease in capillary blood volume Vpc. As inspiration proceeds, the rise in Pel and positive RL, ti$\dot{V}A_o$ (despite lower Ptm_b) causes a net increase in Ppc′. The outflow flow rate exceeds the inlet flow rate, which causes a sharp drop in capillary blood volume (Fig. 4*D*) and a concomitant increase in capillary resistance Rpc (thick line, Fig. 4*B*). At this point, and as $\dot{V}A_o \rightarrow 0$, the effect of Ptm_b on Ppc′ dominates, and Ppc′ falls well into the early part of forced expiration (thin line, Fig. 4*A*). The minimum in Vpc actually occurs past the end of inspiration (Fig. 4*D*).

In the early part of the expiratory phase ($t \geq e^*$), Ppc′ is low, which causes a greater inlet blood flow compared with outflow; the capillary refills quickly to recover its blood volume lost earlier. As expiration proceeds, however, decreasing $\dot{V}A$ increases Ra and Rv, which (despite lowered Rpc) lowers the blood flow rates. Inlet and outlet blood flow rates closely match one another, thereby minimizing variation in Vpc toward the end of the FVC maneuver. Capillary blood volume is also constrained to not exceed Vpc_{max}. The variation in the instantaneous capillary compliance (Cpc) resulting from the nonlinear (sigmoidal-like) shape of the Ptm_b vs. Vpc curve is shown in Fig. 4*E*. Also note the slight

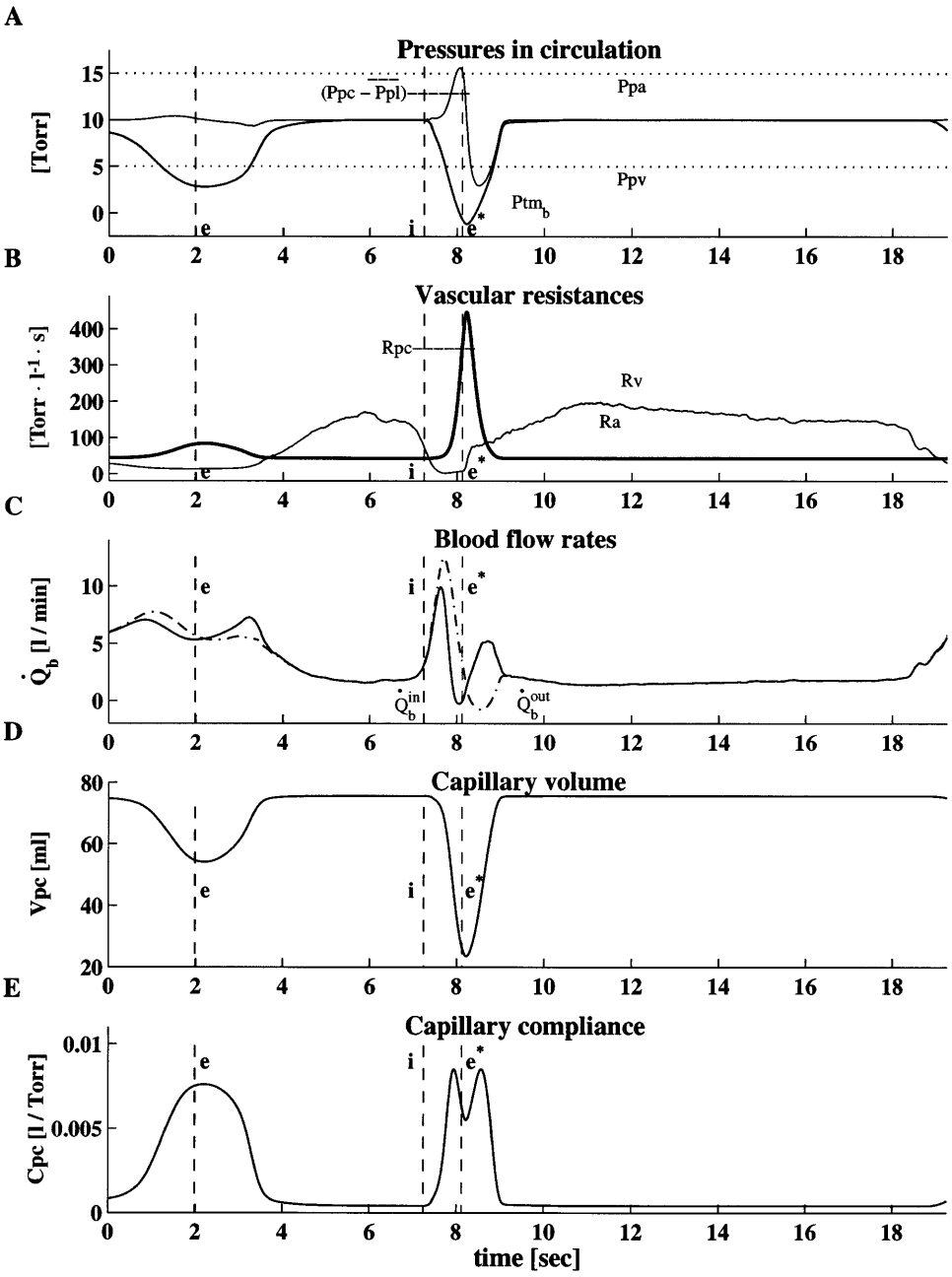

Fig. 4. Pulmonary circulation description during vital capacity maneuver. Vertical dashed lines in all panels are as defined in Fig. 3. *A*: nodal pressures (referenced to $\overline{Ppl}$) and transmural pressure (Ptm_b) across lumped capillary. *B*: pulmonary arterial (Ra), capillary (Rpc), and venous (Rv) resistances. *C*: inlet ($\dot{Q}_b^{in}$) and outlet ($\dot{Q}_b^{out}$) blood flow rates through capillary. *D*: capillary blood volume excursion. *E*: lumped capillary compliance. See *Glossary* for other symbol definitions.

backflow in $\dot{Q}_b^{in}$ and $\dot{Q}_b^{out}$ in the brief instances when $Ppc - \overline{Ppl}$ either exceeds Ppa (zone-1-like behavior) or is lower than Ppv (zone-3-like behavior), respectively, during the transition from inspiration to expiration.

Resistive and Compliant Properties

Figure 5 presents model-generated compliant and resistive properties of the lung and airways for *subject 1* during the FVC maneuver. Figure 5*A* shows the hysteretic behavior associated with Pel, where the lower curve is traversed during inspiration and the upper curve during expiration. The subject's collapsible airway compliance curve is shown in Fig. 5*B*. As Ptm becomes negative during forced expiration, expiratory flow limitation occurs. Figure 5*C* shows the lumped pulmonary capillary exhibiting similar qualitative compliant characteristics.

The effect of VA on Rs is shown in Fig. 5*D*, where the lower curve is traced during inspiration and the upper curve during active expiration (with positive $\overline{Ppl}$). The transition point in the Rs curve during expiration where the slope changes corresponds to a critical volume (V_{crit}; assumed to be 70–80% of FVC), below which the caliber of the peripheral airways is considered to be sensitive to the surrounding positive intrapleural pressure during forced expiration (Fig. 5*D*). Incorporation of this property is purely a modeling construct, necessary to produce the strong concavity observed in the flow-volume loop following peak expiratory flow (e.g., see Figs. 3*A*, 8*A–C*, and 10*A*). RC is

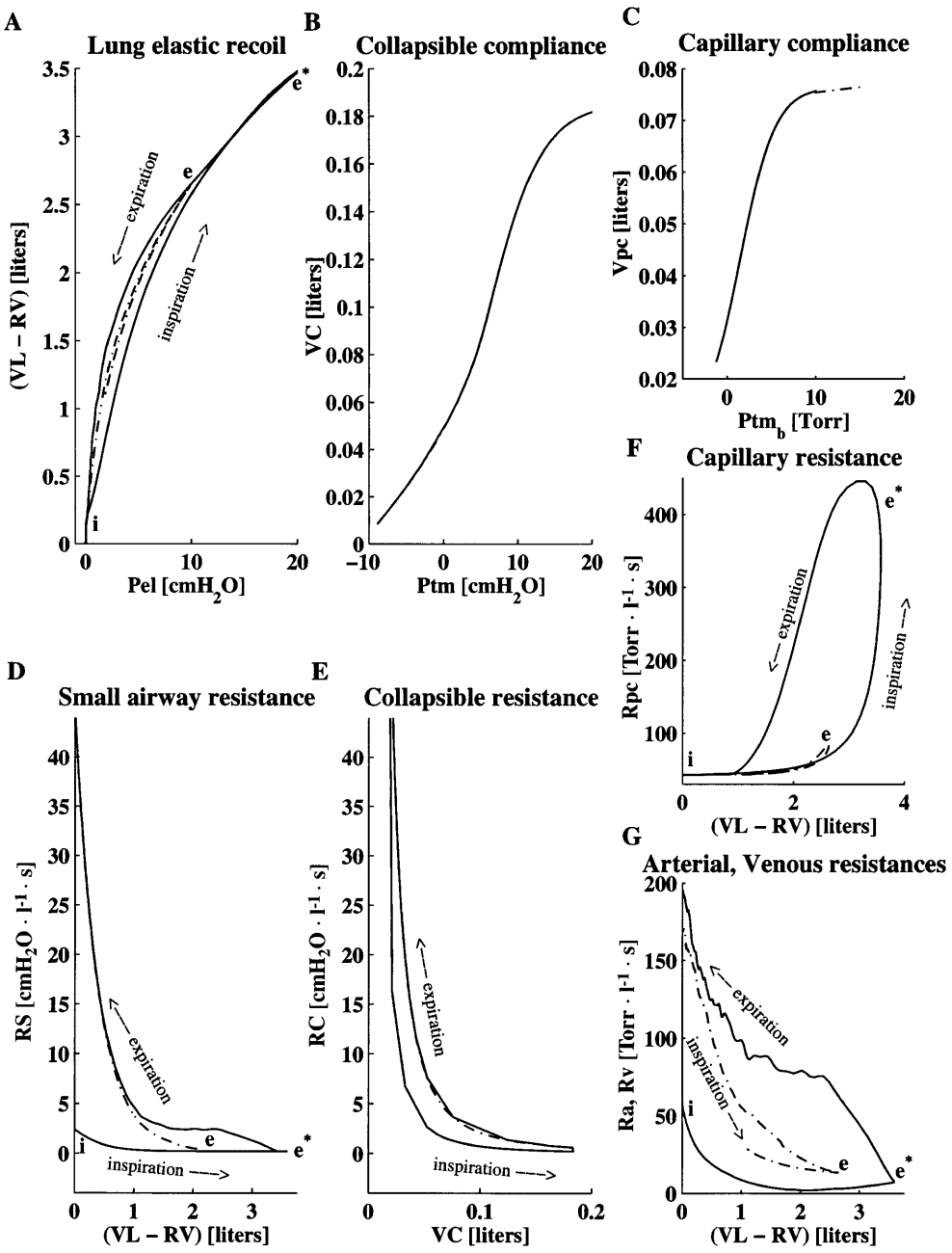

Fig. 5. Description of lung and airway characteristics obtained from parameter estimation for *subject 1*. Dashed-dotted lines corresponds to the episode when subject expired to RV before executing FVC maneuver. Solid line corresponds to when subject executed the FVC maneuver from RV to TLC back to RV. *A*: static lung elastic recoil characteristic. *B*: compliance characteristic of the collapsible airway. *C*: pulmonary capillary compliance characteristic. Note the tapering at higher positive transmural pressures. *D*: excursion in small airway resistance. Note the difference in behavior during positive (forced expiration) and negative (inspiration) $\overline{\text{Ppl}}$ efforts. *E*: resistance variation in collapsible airways. *F*: excursion in pulmonary capillary resistance. *G*: pulmonary arterial and venous resistances. Resistance offered by the capillary region is much greater than that offered by the extra-alveolar arterial and venous resistances. Note the hysteretic behavior exhibited by all the resistances. See *Glossary* for symbol definitions.

similarly described by two curves, traversed differently on inspiration and expiration (Fig. 5*E*). The model-predicted excursions in Rpc, Ra, and Rv shown in Fig. 5, *F* and *G*, agree qualitatively with trends reported in Ref. 37. Clearly, pulmonary vasculature is dominated by transmural effects due to changes in alveolar pressure and the capillary resistance during the FVC maneuver.

Isovolume Pressure-Flow (IVPF) Description

An IVPF curve can be constructed from flow-volume loop data corresponding to various levels of effort (4) and is often used to illustrate expiratory flow limitation. Figure 6 depicts model-generated IVPF curve for *subject 1*. Here, the subject's maximum inspiratory input $\overline{\text{Ppl}}$ (Fig. 3*B*) was scaled to achieve graded lung inflations from RV. Each inflation was followed by forceful expiration with full effort. In addition, with maximal lung inflation from full inspiratory effort, submaximal and supramaximal expiratory efforts were simulated by scaling the positive $\overline{\text{Ppl}}$ record accordingly. Data pairs consisting of predicted airflow rate at the mouth and the corresponding $\overline{\text{Ppl}}$ were separated based on lung volume. The cluster of doublets so obtained then referred to a fixed lung volume (within 1%). Figure 6 shows the results for four lung volumes (1, 2, 2.5, and 3 liters measured from RV; or 27, 54, 68, and 82% of vital capacity). At high lung volumes, a steady increase in expiratory airflow with increasing pleural pressure simulates the effort-dependent expira-

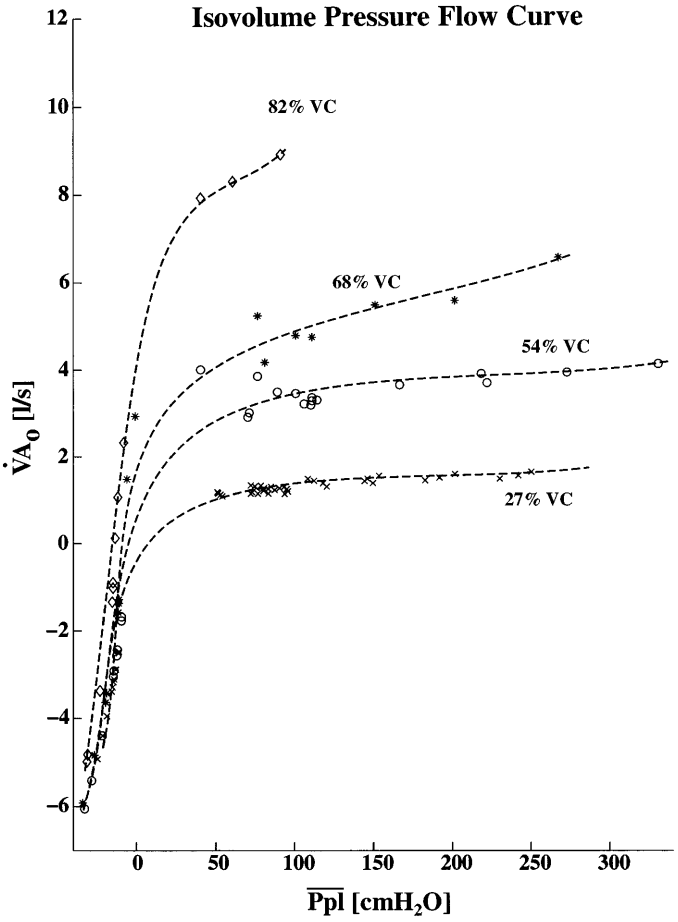

Fig. 6. Isovolume pressure-flow relationship evaluated for *subject 1*. Various levels of expiratory effort were simulated by scaling expiratory intrapleural pressure waveform. Symbols denote simulation results, whereas dashed line was manually traced. VC, vital capacity.

tion characterized by high alveolar elastic recoil. At lower lung volumes, the curve flattens, suggesting a limitation of expiratory flow, regardless of the magnitude of the positive pleural pressure encountered (effort-independent region). Increased dynamic compression of the airways at higher pleural pressures increases peripheral airway resistance contributing to expiratory flow limitation.

Effect of Perfusion on Gas Exchange

Figure 7 compares the temporal profile of expired P_{O_2} and P_{CO_2} observed at the mouth ($P_{E_{O_2}}$ and $P_{E_{CO_2}}$, respectively) for *subject 1* against model predictions for the nominal case (solid line) and for the cases in which the blood flow rate is assumed constant (dashed lines) throughout the maneuver. To provide acceptable fits to the dynamic profiles, it was necessary to have higher blood flow rates during the early part of expiration and lower blood flow rates thereafter. Simulation results assuming fixed blood flow rates (of 1 and 5.4 l/min) are also shown in Fig. 7, *A* and *B*. Clearly, a better fit is obtained with a variable blood flow rate, particularly in the case of the expired CO_2 profile. The relative sensitivity of the CO_2 profile to changes in blood flow rates suggests that CO_2 exchange is more perfusion dependent than is O_2 exchange. Because a single alveolar compartment was employed herein, a change in blood flow rate in effect created a variation in ventilation-perfusion ratio during the course of the FVC maneuver.

Intersubject Variability

Figure 8 shows model-generated fits to the vital capacity maneuver performed by three additional subjects. The same value of RL, ti (0.2 $cmH_2O \cdot l^{-1} \cdot s$) assumed earlier for *subject 1* was utilized for these calculations. Physical input parameters for all four subjects are provided in Table 1, with model parameters obtained from the parameter-estimation algorithm shown in Table 2. There is some difference among the subjects in the actual parameter values obtained. Differences in vital capacity can be attributed in part to differences in the size of the subjects (38); hence, in Fig. 8, lung volumes are shown normalized to body surface area (BSA) instead (assumed to be proportional to the available surface area for gas exchange). Peak expiratory flow rates are comparable for all cases, and the normalized lung volumes lie in the range of 0.33–0.43 ml/cm^2 BSA. Model predictions of the temporal profiles

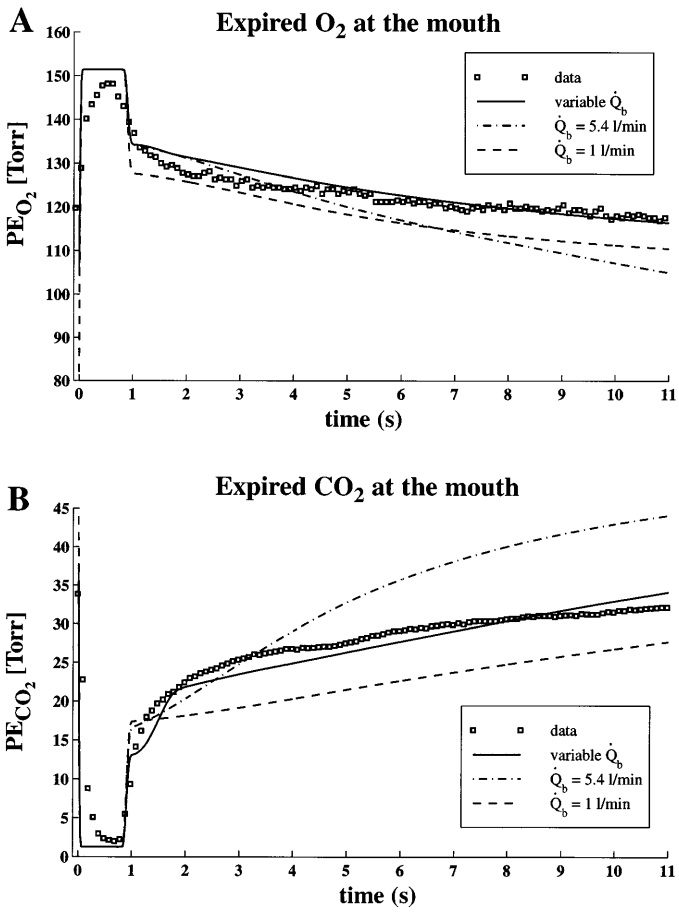

Fig. 7. Effect of changing perfusion rate on expired P_{O_2} and P_{CO_2} in expired gas at mouth during FVC maneuver for *subject 1*. The same $\overline{Ppl}$ corresponding to the reference case (see Fig. 3*B*) was used for all cases presented here. A similar qualitative effect is observed for other subjects (results not shown). *A*: effect on expired O_2. *B*: effect on expired CO_2. See *Glossary* for symbol definitions.

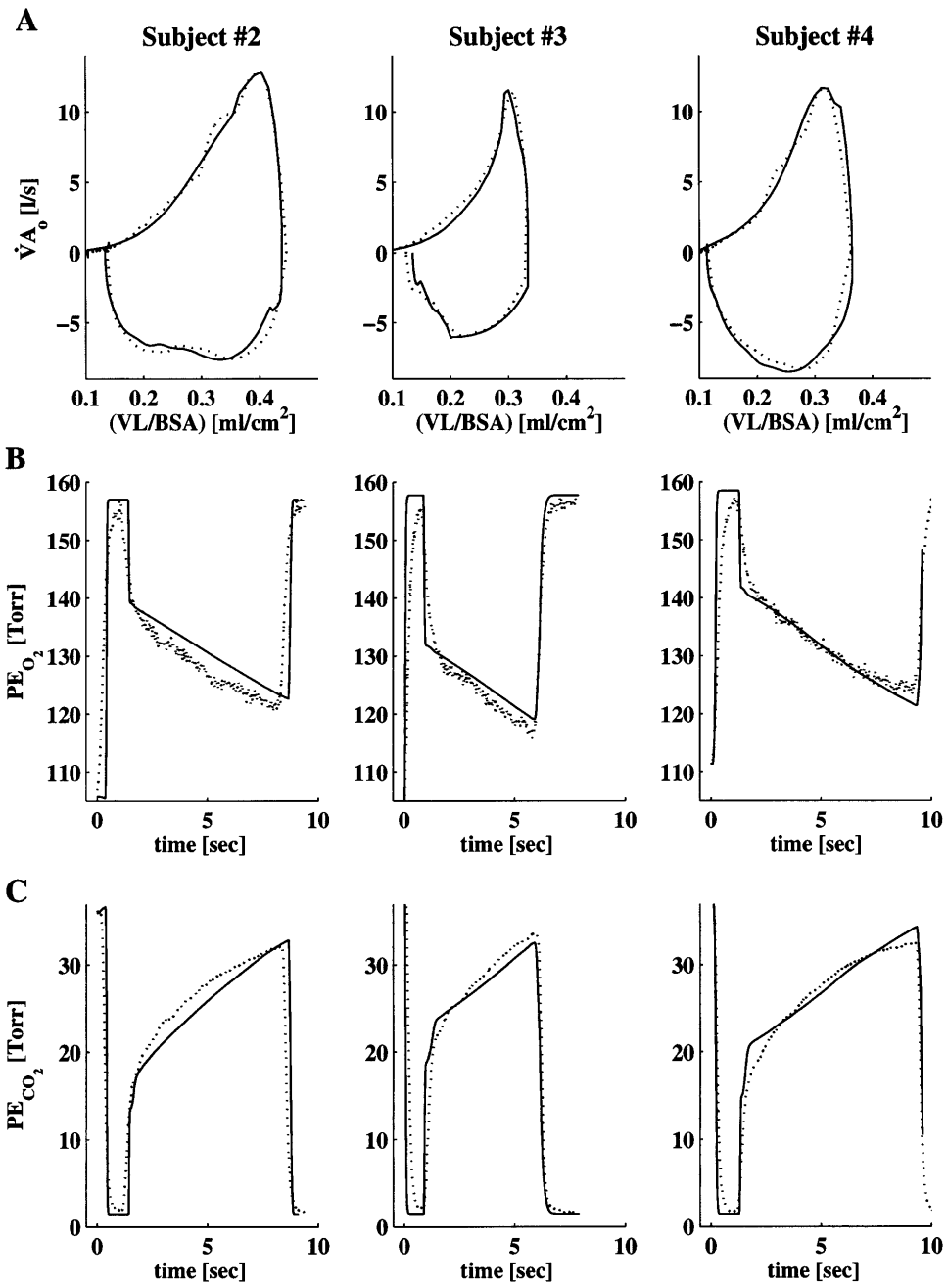

Fig. 8. Comparison of model prediction against data for the VC maneuver performed by 3 other volunteer subjects, provided for reference. Note that volumes are normalized with respect to body surface area (BSA). *A*: flow-volume loops. *B*: time course of expired P_{O_2}. *C*: time course of expired P_{CO_2}. See *Glossary* for symbol definitions.

for O_2 and CO_2 concentrations obtained in the expirate show good agreement with experimental data (second and third rows of Fig. 8). The final end-expiratory P_{O_2} and P_{CO_2} values obtained are comparable despite differences in the individual time histories.

Model-generated spirogram indexes for all four subjects compared against data are depicted in Table 3, again indicating a reasonable agreement for all the subjects and further demonstrating the good fits achieved for the flow-volume loops in general.

Component Resistances

The contributions of component resistances during forced expiration for each of the aforementioned subjects are depicted in Fig. 9, *A–D*. In this case, the expired lung volumes are normalized with respect to vital capacity rather than BSA. In addition, input $\overline{Ppl}$ traces are superimposed on the same plots to indicate the maximum expiratory effort generated by each subject. The general trend in these records indicates that $\overline{Ppl}$ increased linearly with V_L during the initial 10–30% of lung volume during expiration; thereafter, it remains approximately constant, declining only during the last 20% of expiration. The maximum $\overline{Ppl}$ maintained ranged between 90 and 150 cmH_2O. In all cases, over the majority of the volume range, both R_C and Rs far exceed Ruaw (which lies close to the abscissa). At high lung volumes, R_C and Rs are small for all subjects and have comparable effects. The relative contribution of Rs diminishes at lower lung volumes as R_C becomes

Table 2. *Model parameters for volunteer subjects*

Parameter	Units	*Subject 1*	*Subject 2*	*Subject 3*	*Subject 4*
		Upper airway			
K_1	$cmH_2O \cdot l^{-1} \cdot s$	0.31/0.38	0.31/0.38	0.31/0.38	0.31/0.38
K_2	$cmH_2O \cdot l^{-2} \cdot s^2$	0.47/0.46	0.4/0.4	0.32/0.18	0.2/0.16
		Collapsible airway			
K_3	$cmH_2O \cdot l^{-1} \cdot s$	0.2/0.6	0.49/0.45	0.5/0.75	0.24/0.31
Ptm_{max}	cmH_2O	31.4	51.8	71.2	93.9
VC_{max}	liters	0.185	0.125	0.165	0.101
		Alveolar region			
Rs_a		−10.9	−9.9	−6.5	−5.13
Rs_m	$cmH_2O \cdot l^{-1} \cdot s$	2.2/50.2	2.8/90.1	2.47/111.4	5.47/108
Rs_{cmax}	$cmH_2O \cdot l^{-1} \cdot s$	2.35	0.51	1.95	1.18
V*	liters	5.3	10.3	8.41	7.37
V_{crit}	liters	3.39	4.97	3.5	4.17
ξ		3.62	3.55	2.77	1.73
		Pulmonary circulation			
P_ϕ	cmH_2O	37.8	82.2	70.2	50.6
V_ϕ	$cmH_2O \cdot l^{-5} \cdot s$	0.25	0.01	0.02	0.01
Ra_0	$mmHg \cdot l^{-1} \cdot s$	23.6	5.12	25.3	15.7
Rv_0	$mmHg \cdot l^{-1} \cdot s$	23.9	5.3	25.5	15.6
$\underline{R}pc_0$	$mmHg \cdot l^{-1} \cdot s$	57.1	40.2	60.2	55.8
$\overline{C}pc$	l/mmHg	6.9×10^{-4}	2×10^{-4}	2×10^{-4}	0.5×10^{-4}
Vpc_{max}	liters	0.076	0.082	0.072	0.055

Where 2 numbers are shown, value on *left* corresponds to the inspiratory phase (when $\overline{Ppl} < 0$), whereas value on *right* is to be used during forced expiratory phase (when $\overline{Ppl} > 0$). For *subjects 1* and *3*, to accommodate VC_{max} being estimated to be equal or greater than the subject's weight in pounds, an additional 50 ml were included to comprise the anatomical dead space volume [i.e., for *subjects 1* and *3*, $V_D = 50$ ml, else V_D (ml) = body weight (lb.) − VC_{max} (ml)]. See *Glossary* for definitions.

much greater. Both increase, however, as lung volume decreases. Clearly, the behavior of the maximum expiratory flow-volume (MEFV) loop toward the end of the FVC maneuver is dominated by the resistances describing the peripheral and midairways (Rs and R_C, respectively). At high lung volumes, the Ruaw limits the peak expiratory flow rates.

Sensitivity Analysis

The effects of variations in a sampling of the parameters (related to airway/lung mechanics and the pulmonary circulation) on a subset of the model predictions are discussed in this section. Additional calculations (not shown here) were performed to determine the sensitive parameters to be used as candidates in the parameter-estimation algorithm. The intrapleural pressure used as model input corresponds to that generated by *subject 1* during the FVC maneuver (solid line in Fig. 3*B*) and is maintained the same for the simulation study described in this section.

In general, an increase in airway resistance tends to lower peak flow rates as well as impede airflow into and out of the alveolar compartment. The effects are more pronounced during expiration because of the greater magnitude of resistance encountered and are reflected in the expiratory portion of the flow-volume loop. Slower deflation of the lung assists in maintaining lower vascular resistances and increases perfusion, albeit to a very small extent. Because expiration is forceful in this maneuver, the contents of the alveolar compartment are quickly emptied out. Alveolar composition is not significantly affected, thereby resulting in no marked differences in O_2 and CO_2 composition observed at the end of the FVC maneuver. This is unlike during tidal breathing when decrease in the upstroke slope leads to lower end-tidal CO_2 composition. During forced expiration, these small differences

Table 3. *Comparison of spirogram indexes for the subjects*

Spirogram Index	*Subject 1*		*Subject 2*		*Subject 3*		*Subject 4*	
	Data	Model	Data	Model	Data	Model	Data	Model
FEF_{25-75}, l/s	3.22	3.61	5.88	5.55	3.77	4.17	5.79	6.07
FEV_1/FVC, %	77.5	78.1	73.5	72.6	74.9	74.7	71.9	76.4
FEV_3/FVC, %	95.6	99.9	92.1	93.2	95.0	98.8	92.9	99.9
VC, liters	3.67	3.5	6.23	6.58	4.73	4.41	5.29	5.06
PEF, l/s	8.66	8.77	12.8	12.9	11.4	11.5	11.5	11.7
PIF, l/s	6.08	6.12	7.56	7.62	5.99	6.14	8.30	8.54

FEF_{25-75}, forced expiratory flow between 25 and 75% volume; FEV_1 and FEV_3, forced expiratory volume in 1 and 3 s, respectively; FVC, forced vital capacity; VC, vital capacity; PEF, peak expiratory flow; PIF, peak inspiratory flow.

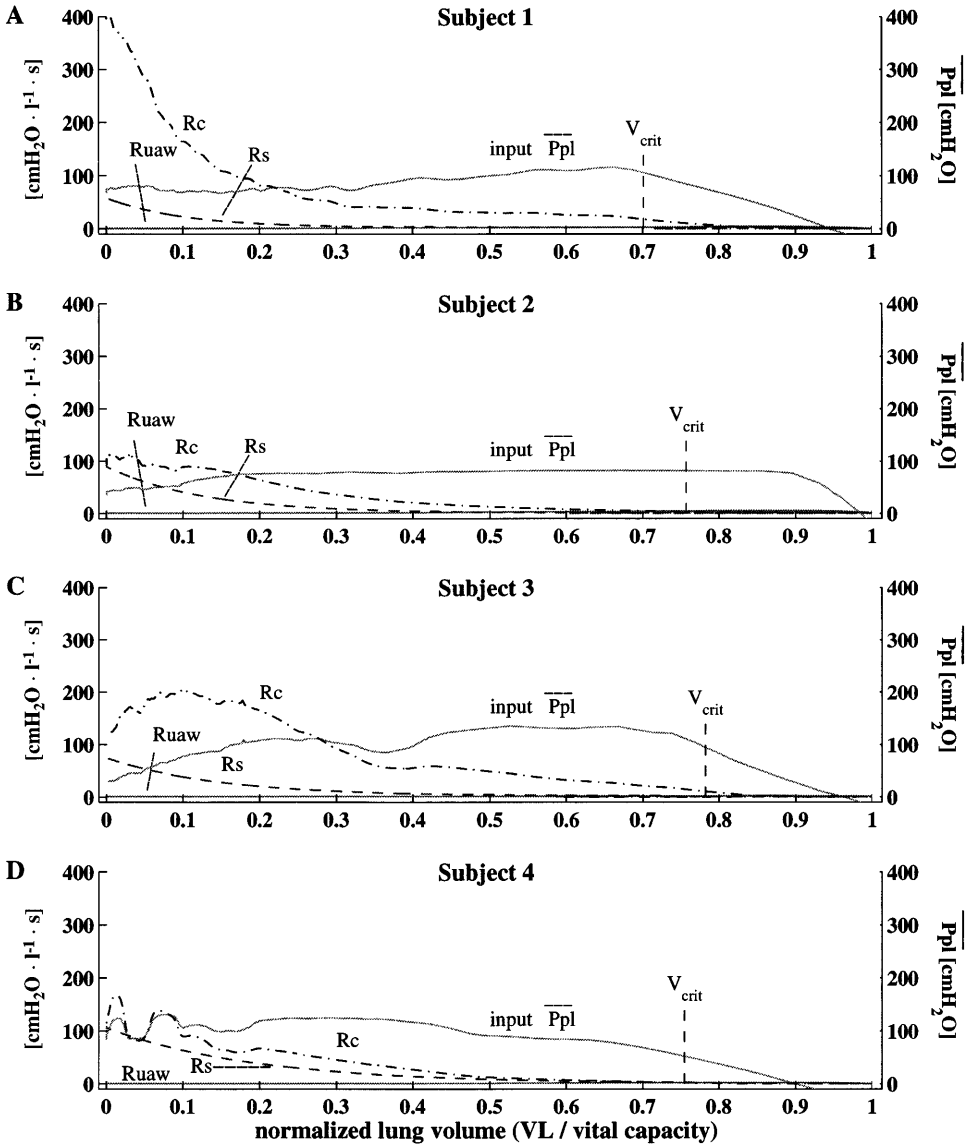

Fig. 9. Contribution of component resistances for the FVC maneuver for all volunteer subjects (*A–D*). Differences in type of effort generated are reflected in variation in $\overline{Ppl}$ in the 4 subjects. Note that Rc dominates beyond peak expiratory flow, whereas effects of Rs are increasingly apparent only at low lung volumes. Upper airway resistance contributes only to peak expiratory flow. V_{crit} occurs toward early part of the forced expiratory phase in all subjects. See *Glossary* for symbol definitions.

are, in general, attenuated, and insignificant effects on expired-gas tracings are observed.

In contrast, alterations in alveolar compliance result in marked variation in resulting lung volume changes for the same intrapleural pressure variation. This causes marked changes in alveolar composition and is reflected in the final levels of gas composition observed in the expired gas. Alveolar composition is dictated by the extent of gas exchange occurring across the alveolar-capillary membrane and is mainly governed by the ratio of perfusion to ventilation. Changes in parameters describing pulmonary circulation cause alterations in perfusion rates which, in turn, modify gas-exchange rates, alter alveolar composition, and significantly affect the time course of the expired-gas composition.

A more detailed sensitivity analysis is conducted by altering the functional descriptors for the resistances and compliances. A summary of the qualitative effects of the individual component parameters and the resulting correlation between model parameters and property attributes of the physiological variables is provided in Table 4. This is useful in eliciting mechanistic insight into resulting system behavior. Detailed illustrations for a sample subset of the parameters listed in Table 4 are depicted in Figs. 10 and 11.

Effect of airway mechanics parameters. SMALL AIRWAY RESISTANCE. Obstructed small airways exaggerate the concavity of the MEFV curve. This is illustrated by adjusting a couple of model construct parameters describing Rs.

1) Effect of Rs_{cmax}. Concavity of the effort-dependent portion of the expiratory flow-volume loop can be reduced by increasing the patency of the small airways. This is equivalent to decreasing Rs_{cmax} in *Eq. 6A* in APPENDIX A. The effect of reducing Rs_{cmax} to 50% of control is shown in Fig. 10*A*, where the resulting flow during expiration is less influenced by positive pleural pressure; hence, less concavity is exhibited in the expiratory flow loop. For reasons explained earlier, the expired CO_2 profile is unaffected (Fig. 10*B*).

Table 4. *Qualitative description of the effects of individual model parameters on functional dependencies for resistances and compliances*

Model Parameter	Functional Dependency	Physiological Variable	Correlation
K_1	Linear portion	Ruaw	Prop
K_2	Quadratic portion	Ruaw	Prop
K_3	Magnitude	R_C	Prop
Ptm_{max}	Stiffness	C_{clp}	Inv
$V_{C_{max}}$	Magnitude	R_C	Prop
Rs_a	Curvature	Rs	Inv
Rs_m	Maximum value at RV	Rs	Prop
Rs_{cmax}	Small-airway patency effort-dependent concavity	Rs	Prop
V*	Maximum possible V_A	C_A	Prop
V_{crit}	Airway caliber reduction	Expiratory Rs	Inv
ξ	Compliance	C_A	Prop
P_ϕ	Curvature based on $\overline{Ppl}$	Ra, Rv	Inv
V_ϕ	Curvature based on V_A	Ra, Rv	Prop
Ra_0	Mean value	Ra	Prop
Rv_0	Mean value	Rv	Prop
$\underline{R}pc_0$	Value at Vpc_{max}	Rpc	Prop
$\overline{C}pc$	Mean value during tidal	Cpc	Prop
Vpc_{max}	Maximum capillary volume	Rpc	Prop

Prop, Proportionality, i.e., increase in model parameter (1st column) would yield an attendant increase in the corresponding physiological parameter (3rd column). Inv, Inverse proportionality, i.e., increase in model parameter (1st column) would cause a resulting decrease in the corresponding physiological parameter (3rd column).

2) Effect of V_{crit}. The abrupt increase in small airway resistance due to reduction in its caliber during the effort-dependent portion of the FVC maneuver below which pleural pressure effects become evident was analyzed by using the nominal parameter, V_{crit} (*Eqs. 5A,a* and *6A* describing Rs_c in APPENDIX A). The value of V_{crit} is assumed to vary among subjects. Delaying the onset of this switching (simulated by decreasing V_{crit} to 50% of control and shown by dashed-dotted line in Fig. 10*A*) produces larger expiratory flow rates for the same lung volume until such time that airway closure becomes dominant. Profile of CO_2 in the expirate is marginally affected.

ALVEOLAR COMPLIANCE. An increase in alveolar compliance (simulated by lowering Pel_{max}; resulting Pel is only 50% of the control value) causes overinflation, thereby increasing vital capacity (dotted line in Fig. 10*C*). The maximum expiratory flow rate achieved is greater than that for the control case. Resulting dilution of alveolar contents consequently results in a lowered value for P_{CO_2} in the airways and is correspondingly reflected in the expired gas at the mouth (dotted line in Fig. 10*D*). Buildup of CO_2 in the expirate is lowered and approaches the final value at a different slope.

COLLAPSIBLE AIRWAY RESISTANCE. The influence of R_C extends throughout the FVC maneuver, as indicated in Fig. 9. An increase in R_C (simulated by doubling K_3 during inspiration and expiration) tends to lower both the inspiratory and expiratory peak flows (dashed line in Fig. 10*C*). Once again, the time course of CO_2 concentration in the expired gas at the mouth is unaffected (dashed line in Fig. 10*D*).

UPPER AIRWAY RESISTANCE. An increase in Ruaw produces significant effects in both lung volumes and airflows. Because the Ruaw is also dependent on flow, the effects of increasing Ruaw (200% of control) are more pronounced, yielding much lower vital capacities and peak inspiratory and expiratory values (dashed-dotted line in Fig. 10*C*).

Effect of vascular parameters. The effect of modifying selected parameters describing the pulmonary vasculature during the FVC is shown in Fig. 11. The flow-volume loop was not affected by the perturbation of the vascular parameters. The control case is depicted by the solid line in Fig. 11. A decrease in the vascular resistances [simulated by setting either Ra_0 (in *Eq. 15A,c*), Rv_0 (in *Eq. 15A,d*), or Rpc_0 (in *Eq. 15A,e*) to 50% of baseline] increases the inlet (Fig. 11, *A* and *D*) and outlet (Figs. 11, *B* and *E*) blood flow rates. This causes a higher CO_2 transfer to the alveolar space and results in higher values of end-expiratory $P_{E_{CO_2}}$ (Fig. 11, *C* and *F*). Because Rpc dominates vascular resistance, reduction of this resistance greatly affects blood flow rates. The coupling between the alveolar volume and extra-alveolar resistances at lower lung volume was investigated through variation of the nominal parameter V_ϕ (*Eqs. 15A,c* and *15A,d*). A reduction in V_ϕ to one-half of its nominal value effectively reduces Ra and Rv, thereby resulting in increased blood flow rates.

Regional parameter sensitivity. The comparative effects of the sensitive model parameters can be localized to specific regions in the flow-volume loop and expired-gas concentration temporal profiles and are schematically depicted in Fig. 12. Regions of the flow-volume loop influenced by the particular parameter during the inspiratory and expiratory phases are shown in Fig. 12*A*. R_C has a dominant effect during most of the FVC maneuver, whereas Rs effects (via model parameters Rs_m and Rs_a) are more evident at lower lung volumes. The drop in airflow following expiration is mainly dictated by V_{crit} and Rs_{cmax} (parameters that affect Rs). Ruaw strongly influences peak inspiratory and expiratory flow rates as well as the initial upstroke in forced expiration. Parameters describing compliance of the collapsible segment (Ptm_{max} and $V_{C_{max}}$) and the alveolar region (ξ and V*) affect the inspiratory phase. Effects of parameteric changes on the flow-volume loop are also reflected in the expired-gas composition profile, as shown in Fig. 10, *B* and *D*.

Figure 12*B* shows the model parameters that significantly affect the FVC capnogram ($P_{E_{CO_2}}$). The initial upstroke in CO_2 tension in the expirate remains unaffected. The initial peak attained is affected by pulmonary capillary compliance (Vpc_{max}, $\overline{C}pc$) and resistance (Rpc_0). The ramplike increase in the temporal profile is influenced by the arterial and venous resistive parameters (Ra_0, Rv_0, V_ϕ, and P_ϕ). Note, however, that end-expiratory compositions so obtained depend on the cumulative effect of all the parameters.

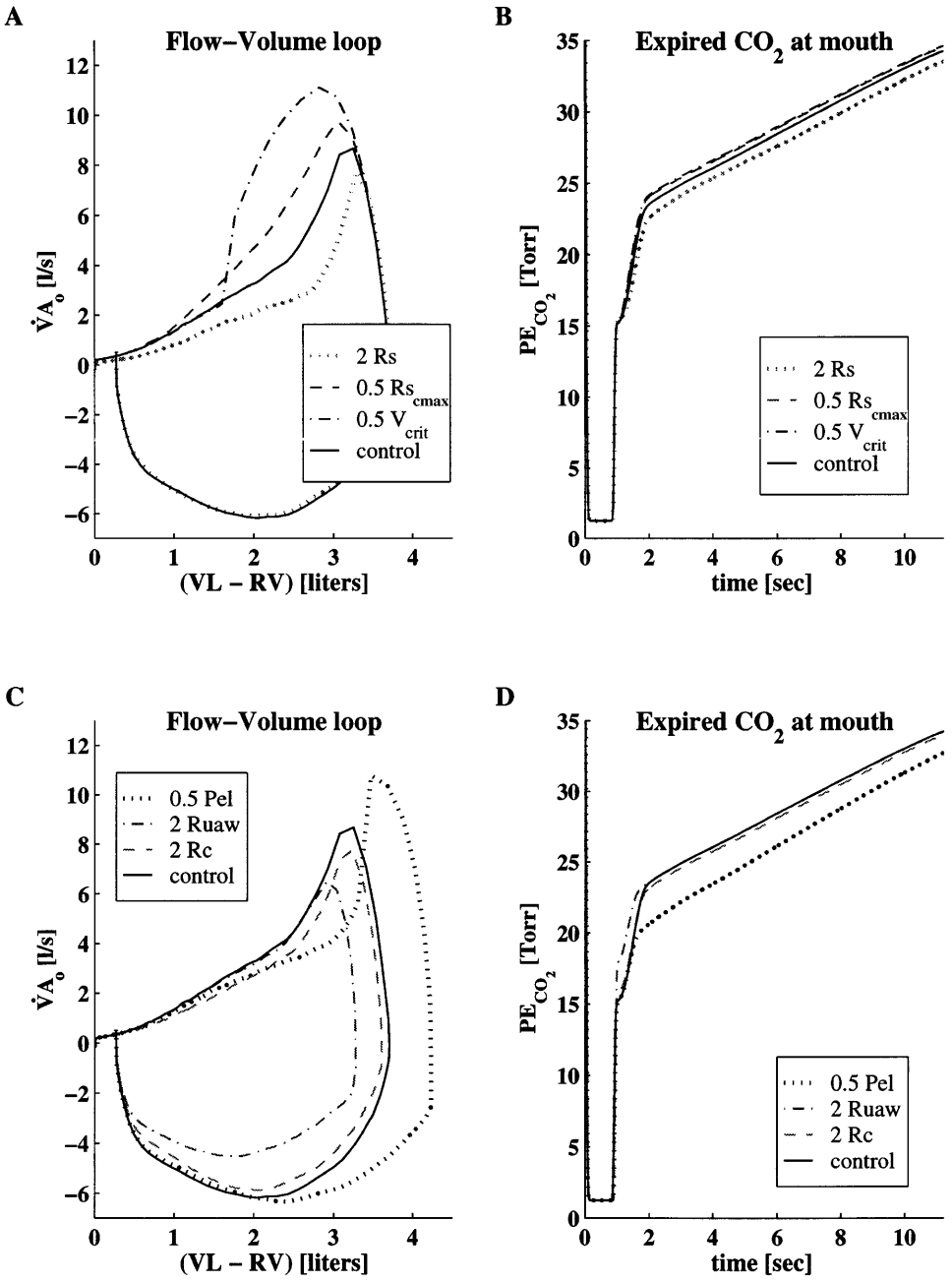

Fig. 10. Effect of airway mechanics parameters during FVC. Parameters describing *subject 1* were used as baseline for all cases. For each scenario, only 1 of parameters was modified while all others were unchanged. Same driving intrapleural pressure (shown in Fig. 3*B*) was used in all cases. *A* and *C*: effect on flow-volume loop. *B* and *D*: effect on P_{CO_2} at the mouth during forced expiration. See *Glossary* for symbol definitions.

DISCUSSION

To develop a mathematical model that emulates the functional behavior of the respiratory system, it is essential to characterize the airways and lung and alveolar-capillary gas transport. The lumped model presented consists of nonlinear resistive-compliant airway and alveolar compartments interacting with pulmonary vascular compartments. Measured pleural pressure was used to drive the model, and a nonlinear parameter-estimation scheme was employed to identify model parameters that yielded good agreement between model predictions and experimental data. The FVC maneuver was chosen to illustrate the excursion over the full range of permissible lung volumes. After the system under the vital capacity maneuver has been identified, it should be possible to predict its behavior during other breathing maneuvers, i.e., tidal breathing and panting, holding the parameter set unchanged (not shown here).

Airway/Lung Mechanics

The $\overline{Ppl}$ waveform measured during the FVC maneuver differed among subjects but was characterized by a sharp transition between initial maximal inspiratory and expiratory efforts, followed by a prolonged positive offset beyond the point when peak expiratory flow was achieved. The curve showing $\overline{Ppl}$ as a function of lung volume (Fig. 9, *A–D*) clearly demonstrates that the flow work ($\int \overline{Ppl}\, dV_L$) developed by individual subjects differed during the forced expiratory period. To simu-

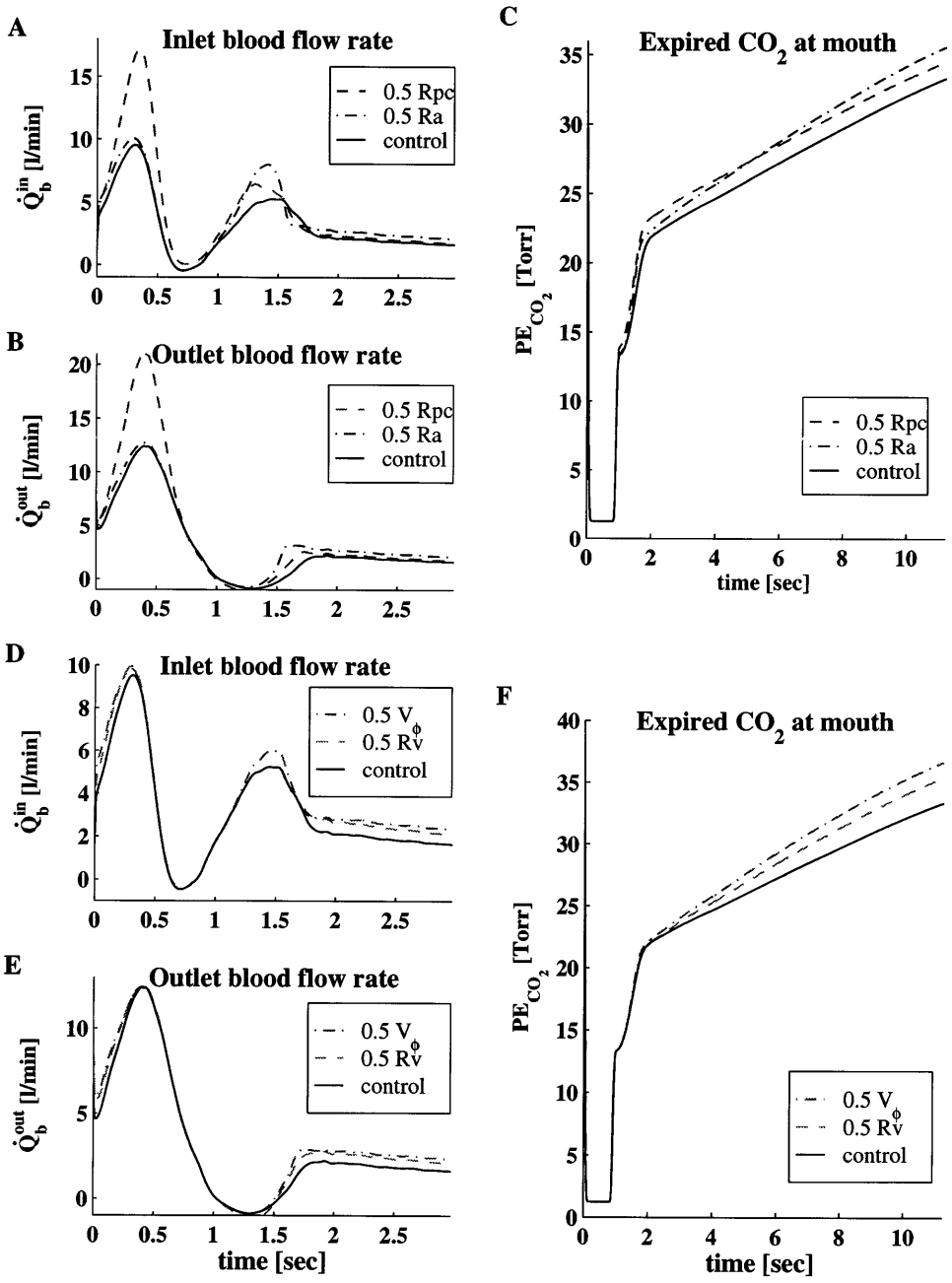

Fig. 11. Effect of modifying vascular parameters during FVC. Parameters describing *subject 1* were used as baseline for all cases. For each scenario, only 1 of parameters was modified while all others were maintained unchanged. Same driving intrapleural pressure (shown in Fig. 3*B*) was used in all cases. *A* and *D*: effect on inlet blood flow rate. *B* and *E*: effect on outlet blood flow rate. *C* and *F*: effect on P_{CO_2} at the mouth during forced expiration. See *Glossary* for symbol definitions.

late zero flow at the mouth toward the end of the FVC maneuver, it was necessary to assume high airway resistance at low lung volumes (Figs. 5, *D* and *E* and 9*A–D*), in effect simulating progressive airway closure toward end expiration (32, 33, 39). An increase in airway resistance at low lung volumes via elevation of Rs alone can also produce this effect on the flow-volume loop (13, 14), but it creates significant discrepancies between model predictions and experimentally measured data corresponding to the time course of P_{O_2} and P_{CO_2} values observed in the expired gas. Large values of Rs did not permit efficient transport of gases from the alveolar region to the mouth, and underpredicted P_{CO_2} and overpredicted P_{O_2} values in the expired gas (at end expiration). It was, therefore, necessary to allocate the resistance changes at low volumes to both Rs and Rc, to achieve reasonable fits to all aspects of the data. Figure 9 again demonstrates the importance of the collapsible segment during the FVC maneuver. Simulation results presented here suggest that the contribution of Rc during the latter part of forced expiration is greater than any of the other component airway resistances.

To obtain concavity of the flow-volume loop past peak expiratory flow, it was necessary to incorporate two parameters, V_{crit} and Rs_{cmax}, which describe the abrupt increase in Rs due to the effects of positive $\overline{Ppl}$ (Fig. 5*D*). V_{crit} corresponds to a critical lung volume below which this effect is apparent. The increase in magnitude in Rs when lung volume equals V_{crit} is then characterized by Rs_{cmax} (Eq. 6*A*).

Pulmonary Circulation

In this work, it was found necessary to include a time-varying description of the pulmonary blood flow

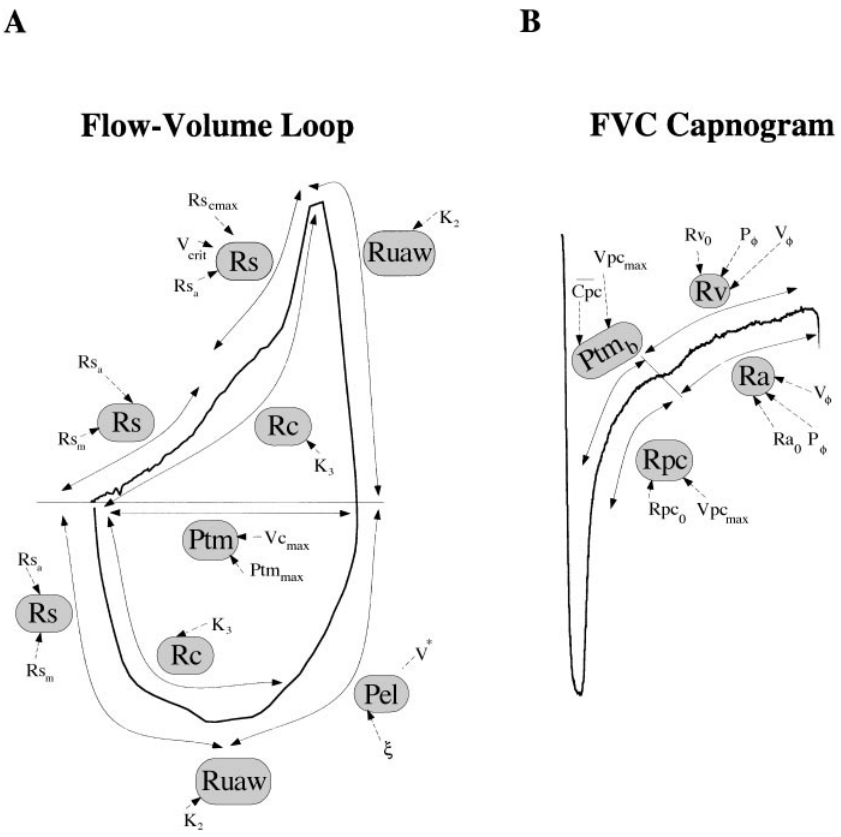

Fig. 12. Schematic representation of localization of contribution of model parameters to flow-volume loop and FVC capnogram (expired P_{CO_2} in expired gas at mouth during FVC maneuver). *A*: effect on flow-volume loop. *B*: effect on expired CO_2 waveform at mouth. See *Glossary* for symbol definitions.

rate to obtain gas-exchange predictions that were consistent with experimental observations on the time course of $P_{E_{O_2}}$ and $P_{E_{CO_2}}$. The model presented includes the externally imposed effects of alveolar volume and alveolar and intrapleural pressures. The effects on the extra-alveolar and intra-alveolar volumes are dissimilar. The model is capable of simulating capillary recruitment-derecruitment in terms of changing capillary blood volume for the breathing maneuver considered (Fig. 4*D*). The prediction is qualitatively consistent with observations reported in the literature during tidal breathing in terms of the direction of changes in blood volume (37). The dynamics of changes in pulmonary blood flow rate determine O_2 influx and CO_2 excretion.

Gas Exchange

An adaptive pulmonary circulation model has also been included in addition to an air-side model to describe gas exchange at the alveolar-capillary membrane. Dynamic interaction of air-side variables with the pulmonary circulation variables clearly affects capillary gas exchange. For instance, blood flow rate through the pulmonary capillary is governed by the pulmonary vasculature resistances, which, in turn, depend on alveolar volume and pleural pressure. Hence, they exhibit variations throughout the phase of the respiratory cycle that affects the residence time of blood in the capillary bed. Changes in forward and retrograde blood flow produced during forced inspiration are responsible for the nature of the early profile of P_{CO_2} in the expired gas. Use of constant pulmonary capillary blood flow rate did not match the early phase of the expired CO_2 time course (Fig. 7). This coupled aspect of pulmonary airway/lung mechanics, circulation, and gas exchange has not been included in previously reported mathematical models.

Model Limitations

Although the model presented in this work is quite detailed, like all mathematical models, it must be considered in the context of known limitations.

1. The performance of the model in tracking expiratory behavior at submaximal inspiratory effort as well as at low lung volumes (near RV) is less than satisfactory (Fig. 3, *A* and *D*). Improvements in better emulation of airway closure are warranted.

2. Distributed-parameter models based on morphometric representations of the airways (57) have been employed to simulate expiratory flow limitation by using wave-speed mechanisms (10, 25, 53). Wave phenomena cannot be addressed by using lumped models. Herein flow limitation is attributed solely to viscous dissipation.

3. In general, subjects with respiratory system abnormalities often tend to have regional dysfunction (39). These regional differences can hinder gas-transport efficiency in a nonuniform, heterogeneous fashion, which suggests that the one-compartment approach applied here to normal subjects would not be adequate for characterizing patients with airway disease. The model has obvious limitations in characterizing diseased subjects. To simulate airway disease, it would be necessary to partition the alveolar compartment into multiple

subcompartments with variable regional ventilation and perfusion. This would significantly increase model complexity, and validation of the expanded model would require additional measurements on regional ventilation and perfusion. Because conventional clinical pulmonary function laboratories are often limited to minimally invasive procedures, a trade-off exists between model complexity and the number and types of pulmonary variables that can be monitored with conventional measurement techniques. It has been suggested in the literature that ventilation inhomogeneity associated with lung disease can be examined by incorporating an insoluble gas, e.g., Ar, to help distinguish the effects of nonuniform ventilation and capillary gas exchange (45). This approach, which reportedly does not require the use of additional compartments, needs to be further explored. A point worth investigating, however, is the degree to which reduced, lower order models (including this single-lung-compartment model with altered characteristics) are capable of capturing the essential dynamic features of the complete system. These lower order models, although less accurate, require fewer measurements for model validation and yet provide useful insights into the potential interaction between ventilation and pulmonary blood flow.

4. The sloping capnogram (shown in Fig. 7) was characterized by incorporating time-varying blood flow rate. The effect of including multiple compartments with varied ventilation and perfusion levels (as mentioned above) to generate the desired time-course description of the expired gases was beyond the scope of the present study.

5. Airway inertance is assumed to be negligible at normal respiratory frequencies (39). Ignoring inertial effects may not be leading to accurate results during the early part of forced expiration, which is characterized by high airflows. Depending on the specific application, an inertance might need to be incorporated between the upper airway resistance and the collapsible segment in Fig. 1*B*. Inertance would be mandatory for analysis of high-frequency ventilation (11).

6. Lung tissue resistance, R_L, ti, assumed to be constant for all the subjects during the FVC maneuver, ignores stress relaxation (24, 51) in lung tissue.

7. The static lung relaxation curve is dependent on breathing frequency and history (4, 39). As breathing frequency increases, one would expect the relaxation curve to flatten, resulting in a stiffer (lower compliance) characterization of the lung. This aspect is not considered in the present model formulation.

8. The lumped description of the pulmonary circulation presented here is oversimplified. Differences in regional perfusion due to the gravitationally induced changes in hydrostatic pressure [zones 1, 2, and 3 (39, 59)] are not considered. The use of constant-pressure sources to describe the pulmonary arterial and pulmonary venous pressures ignores the dynamic aspect of the pulmonary circulation (the result of right ventricular and left atrial pumping) and the compliant properties of the extra-alveolar vessels. These aspects were neglected because of our present limitation regarding measurement of pulmonary hemodynamic data via indirect means. Obtaining measurements of blood flow during respiratory maneuvers (e.g., utilizing ultrasonic methods) would greatly enhance the ability to identify the appropriate structure for an adequate pulmonary circulation model and the values of associated parameters. Modulation of the pulmonary vascular resistance by the O_2 tension in blood (37, 39) has also been neglected.

9. The open-loop model as formulated is not driven by the metabolic demands of the tissues. The metabolic requirements of O_2 and CO_2 by the tissues cause a corresponding change in the mixed venous gas tensions entering the pulmonary circulation, especially when long breathing episodes are considered as part of any breathing maneuver. The ramifications of artificial panting could be quite different physiologically from those caused by demand panting.

10. During the experimental protocol, the volunteer subjects were allowed to rest between episodes while the capnogram recovered to nominal values. Nevertheless, it is quite possible that during the experiment mixed venous tensions varied from the constant values assumed here. Additional noninvasive measurements of blood gases would yield important new information, and prove useful in providing better model-based assessment of blood-gas concentrations in the pulmonary capillary and gas transport across the alveolar capillary membrane.

Summary

Despite these stated limitations, the lumped nonlinear one-compartment model of airway/lung mechanics, pulmonary circulation, and gas exchange presented in this study satisfactorily describes the dynamics of the FVC maneuver in normal human subjects. The study also demonstrated the feasibility of employing parameter-identification techniques to match experimental data obtained noninvasively in the pulmonary function laboratory. The model serves as a template for future development of other single- and multiple-compartment models that describe abnormalities in pulmonary function. It also serves as a framework to investigate cardiopulmonary interactions. Results indicate that an accurate characterization of the interaction between ventilation and perfusion is essential to achieve satisfactory match to expired O_2 and CO_2 concentration waveforms when using a single-compartment model. As a result of this interaction, the model predicts a steep decline in transient blood flow rates during the execution of the FVC maneuver; this could have clinical consequences under pathophysiological abnormalities. However, such putative changes in pulmonary blood flow rate during the FVC maneuver need to be verified experimentally.

To characterize the inspiratory and expiratory flow-volume loops, it was necessary to incorporate a hysteretic description of airway resistances. Airway resistance values encountered during expiration exceeded

those calculated during inspiration for the same compartmental volume. Specifically, during expiration, significant elevation in both the collapsible midairway and small airway resistances was necessary to adequately characterize the shape of the expiratory flow-volume loop and time course of the FVC capnogram.

Although it provides a quantitative and theoretical basis for physiological interpretation, the model, in its present form, is not expected to be utilized clinically. Even though the model has limitations, nevertheless, it provides useful insight in assessing the inherent coupling between airway mechanics and pulmonary blood flow and the resulting effects on the output variables characterizing gas exchange.

APPENDIX A

Modeling equations were developed by employing macroscopic balances on the overall mass, overall linear momentum, and the species mass by using a control volume approach. Air is assumed to behave ideally with its overall mass density (ρ) being defined by a constitutive equation of state corresponding to the ideal gas law ($P = \rho RT/M$), where T is absolute temperature, M is the molecular weight of air, and R is the universal gas constant. The molecular weight of air is assumed to be invariant to changes in composition in the ensuing formulation. Blood is considered to be incompressible and behave as a homogeneous one-phase mixture.

Mechanics

Air side. PRESSURE WITHIN AIRWAY COMPARTMENTS. The total pressures in the alveolar and collapsible regions at any time, denoted by P_A and P_C, respectively, in Fig. 1, are described by the balance of applied and developed pressures across their respective wall boundaries [D'Alembert principle, (31)] and are written as

$$P_A = Pel + R_L, ti\left(\frac{dV_A}{dt}\right) + \overline{Ppl} + P_{ref} \qquad (1A,a)$$

$$P_C = Ptm + \overline{Ppl} + P_{ref} \qquad (1A,b)$$

where P_{ref} is the reference pressure at 37°C.

The minimum and maximum values of $\overline{Ppl}$ achieved during the vital capacity maneuver with full effort are denoted by Ppl_{min} and Ppl_{max}, respectively. The static P-V relationship for the alveolar compartment, $Pel(V_A, \overline{Ppl})$, is characterized by two curves, Pel^E and Pel^I, which delineate the outer boundaries of the Pel envelope. The Pel^I and Pel^E curves illustrated in Fig. 13*A* are generated by assuming that $\overline{Ppl}$ was held constant at Ppl_{min} (marked $X^{\#} \rightarrow X$ in Fig. 13*B*) and Ppl_{max} (marked $Y \rightarrow Y^{\#}$ in Fig. 13*B*) throughout the inspiratory and expiratory phases, respectively. The mean of these two curves refers to an equilibrium curve corresponding to the case where $\overline{Ppl} = Ppl_{mean}$ (= −3 to −5 cmH_2O typically obtained at end-tidal conditions). The recoil pressure Pel is assumed to be graded according to effort; hence Pel is computed via linear interpolation based on the actual $\overline{Ppl}$ recorded. Interpolation is performed by grading between the equilibrium curve and the Pel^I curve for the inspiratory phase, whereas the equilibrium curve and the Pel^E curve are used for the expiratory-phase. The resulting trace is a hysteretic loop contained within the envelope defined by Pel^I and Pel^E. This, in effect, defines the actual P-V relationship generated for a given subject specific to the $\overline{Ppl}$ recorded while executing the FVC maneuver. The resulting set of equations is then given by

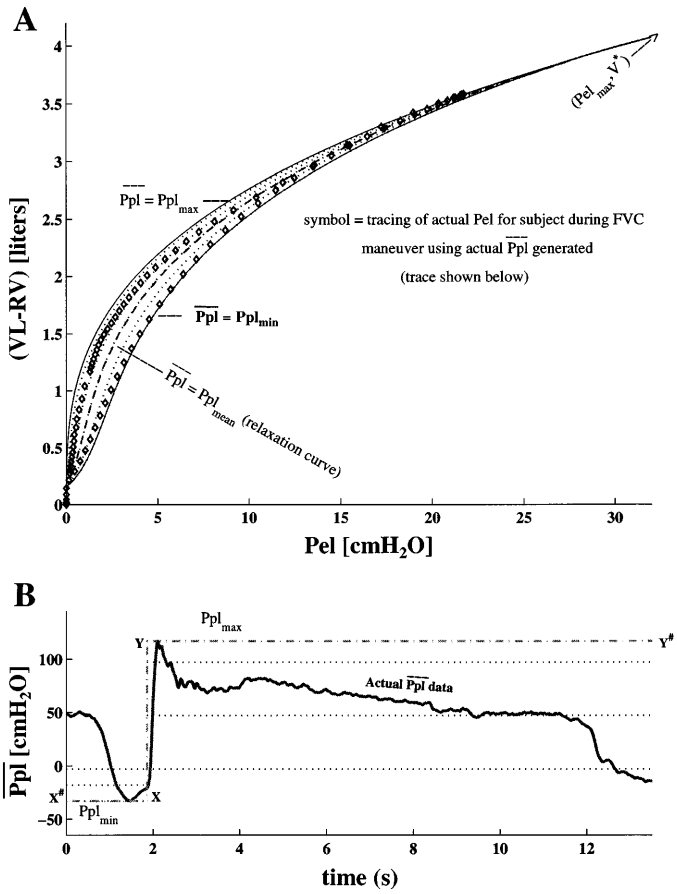

Fig. 13. Generation of static recoil pressure tracing for a given subject. *A*: reference curves by using constant Ppl_{min} and constant Ppl_{max} defined the outer Pel envelope (solid lines in *A* and dashed-dotted line $X^{\#}XYY^{\#}$ in *B*). Dotted lines correspond to recoil pressure at graded levels (illustrated in *B*) of $\overline{Ppl}$. Actual Pel tracing corresponding to *subject 1* during FVC is denoted by ◇ (Pel^I and Pel^E). *B*: actual intrapleural pressure generated by *subject 1* during FVC maneuver shown by solid line. Dotted lines are isobars and depict graded levels of set $\overline{Ppl}$ used during inspiratory and expiratory phases to generate corresponding traces within the Pel envelope shown in *A*.

$$na = \frac{V^* - RV + 0.1}{V^* - RV + 0.001} - 0.99 \qquad (2A,a)$$

$$nb = \frac{V^* - RV + 0.1}{V_A - RV + 0.001} - 0.99 \qquad (2A,b)$$

$$nc = \frac{V^* - RV + 0.1}{0.001} - 0.99 \qquad (2A,c)$$

$$nd = \frac{Pel_{max} + 25}{\ln\left(\frac{nc}{na}\right)} \qquad (2A,d)$$

$$Pel^E = Pel_{max}\left(\frac{V_A - RV + 0.001}{V^* - RV + 0.001}\right)^3 \qquad (2A,e)$$

$$Pel^I = \frac{(\xi Pel^E)\left[Pel_{max} + nd \ln\left(\frac{na}{nb}\right)\right]}{\xi + 1} \qquad (2A,f)$$

$$ne = \frac{0.5}{\mathrm{Ppl}_{mean} - \mathrm{Ppl}_{min}} \quad [\mathrm{Ppl}_{mean} - \overline{\mathrm{Ppl}}(t)] \quad \text{for inspiration} \tag{2A,g}$$

$$ne = \frac{0.5}{\mathrm{Ppl}_{mean} - \mathrm{Ppl}_{max}} \quad [\mathrm{Ppl}_{mean} - \overline{\mathrm{Ppl}}(t)] \quad \text{for expiration} \tag{2A,h}$$

$$\mathrm{Pel} = (0.5 + ne)\,\mathrm{Pel}^{E} + (0.5 - ne)\,\mathrm{Pel}^{I} \quad \text{for expiration} \tag{2A,i}$$

$$\mathrm{Pel} = (0.5 - ne)\,\mathrm{Pel}^{E} + (0.5 + ne)\,\mathrm{Pel}^{I} \quad \text{for inspiration} \tag{2A,j}$$

where Pel_{max} (>0) is the magnitude of the minimum $\overline{\mathrm{Ppl}}$ obtained during maximal inspiratory effort; and V* and ξ are parameters describing Pel and are determined for each subject through the parameter-estimation algorithm.

The transmural pressure across the collapsible compartment, Ptm, is expressed as a function of VC (40) and is given as

$$lbptm = \frac{(\mathrm{Ptm}_{max} - 5.6)}{6.908} \tag{3A,a}$$

$$\mathrm{Ptm} = saptm - sbptm\left(\frac{\mathrm{VC}}{\mathrm{VC}_{max}} - 0.7\right)^2 \quad \text{if} \quad \frac{\mathrm{VC}}{\mathrm{VC}_{max}} \le 0.5 \tag{3A,b}$$

$$\mathrm{Ptm} = 5.6 - \left[lbptm \ln\left(\frac{\mathrm{VC}_{max}}{\mathrm{VC}} - 0.999\right)\right] \quad \text{if} \quad \frac{\mathrm{VC}}{\mathrm{VC}_{max}} > 0.5 \tag{3A,c}$$

where VC_{max} again is a parameter determined for each subject using the estimation algorithm; and *saptm* and *sbptm* are constants determined by forcing continuity and differentiability of Eq. *3A,b* and *3A,c* at $\mathrm{VC}/\mathrm{VC}_{max} = 0.5$.

FLOW BETWEEN AIRWAY COMPARTMENTS. All flows are evaluated at body temperature (T_{body}). Equations describing the flows beteen the collapsible and alveolar regions ($\dot{Q}_{CA}$), between the dead space and the collapsible airway ($\dot{Q}_{DC}$), and in the upper airway ($\dot{Q}_{ED}$), are derived from the balance on overall linear momentum in each region. Ignoring the inertial contributions, the expressions for flow are given as

$$\dot{Q}_{CA} = \frac{P_C - P_A}{Rs} \tag{4A,a}$$

$$\dot{Q}_{DC} = \frac{P_D - P_C}{R_C} \tag{4A,b}$$

$$\dot{Q}_{ED} = \frac{P_{ref} - P_D}{Ruaw} \tag{4A,c}$$

The small airway resistance Rs has different values for the two respiratory phases. The value for Rs during expiration is greater than that during inspiration for the same lung volume because of the effects of airway closure during forced expiration. The expressions for RC and Ruaw are similar to those listed elsewhere (40, 44). The various airway resistances are thereby given as

$$Rs = Rs_m \exp\left(Rs_a \frac{V_A - RV}{V^* - RV}\right) + Rs_c \tag{5A,a}$$

$$R_C = K_3\left(\frac{\mathrm{VC}_{max}}{\mathrm{VC}}\right)^2 \tag{5A,b}$$

$$Ruaw = K_1 + K_2|\dot{Q}_{ED}| \tag{5A,c}$$

Note that Rs_c is held constant at 0.02 when $\overline{\mathrm{Ppl}}$ is negative. However, when $\overline{\mathrm{Ppl}}$ exceeds zero (e.g., during forced expiration) and when VL is below a critical volume [V_{crit}, ~70–80% of vital capacity (VC)], the resistance to airflow offered by the small airways is assumed to be a function of effort resulting in increased Rs. This aspect is modeled by defining Rs_c to be effort dependent according to

$$Rs_c = \frac{Rs_{c\,max} - 0.02}{\mathrm{Ppl}_{max}}(\overline{\mathrm{Ppl}} - \mathrm{Ppl}_{max}) + Rs_{c\,max} \tag{6A}$$

Airflow detected by the flow transducer located within the mouthpiece is designated as $\dot{V}_{A_o}$. Model-generated flow at the mouth is calculated according to

$$\dot{V}_{A_o} = \dot{Q}_{ED}\frac{T_{am}}{T_{body}}\frac{(P_{ref} - P_{H_2O|T_{body}})}{P_{ref}} \quad \text{for inspiration}$$
$$\dot{V}_{A_o} = \dot{Q}_{ED} \quad \text{for expiration} \tag{7A}$$

VOLUME CHANGES IN THE COMPLIANT AIRWAY COMPARTMENTS. Invoking overall continuity (conservation of total mass) in the two compliant compartments, the dynamic expressions for the rate of change of volume in the compartments may be written as

During inspiration

$$\frac{dV_C}{dt} = \left(\frac{\rho_D}{\rho_C}\right)\dot{Q}_{DC} - \dot{Q}_{CA} - \left(\frac{V_C}{\rho_C}\right)\frac{d\rho_C}{dt} \tag{8A}$$

$$\frac{dV_A}{dt} = \left(\frac{\rho_C}{\rho_A}\right)\dot{Q}_{CA} - \left(\frac{V_A}{\rho_A}\right)\frac{d\rho_A}{dt} - \left(\frac{P_S T_{body}}{T_S P_A}\right)\Phi^*_{tot} \tag{9A}$$

During expiration

$$\frac{dV_C}{dt} = -\dot{Q}_{DC} - \left(\frac{\rho_A}{\rho_C}\right)\dot{Q}_{CA} - \left(\frac{V_C}{\rho_C}\right)\frac{d\rho_C}{dt} \tag{10A}$$

$$\frac{dV_A}{dt} = -\dot{Q}_{CA} - \left(\frac{V_A}{\rho_A}\right)\frac{d\rho_A}{dt} - \left(\frac{P_S T_{body}}{T_S P_A}\right)\Phi^*_{tot} \tag{11A}$$

where Φ^*_{tot} is the total gas exchange of all species considered from the alveolar region to the blood in the capillary across the alveolar-capillary barrier, and is given as

$$\Phi^*_{tot} = \sum_{i=1}^{N_{tot}}\sum_{j=1}^{N_{seg}}\frac{D_{L_i}(P_{A_i} - Pb_i^{(j)})\Delta Vpc^{(j)}}{Vpc} = \sum_{i=1}^{N_{tot}}\phi_i \tag{12A}$$

The inner summation represents the total transfer rate (STPD) of species *i* across the capillary wall, ϕ_i, and is evaluated by summing the transfer across each of the discretized capillary segments *j*. $\Delta Vpc^{(j)}$ denotes the volume of the *j*th capillary segment. Note that *Eqs. 9A* and *11A* when expanded result in a second-order ordinary differential equation and can be alternately expressed as two first-order ordinary differential equations using state companion form (19).

Application of overall continuity in the rigid dead-space region results in a dynamic expression for the total density in the dead space and is given by

$$\frac{d\rho_D}{dt} = \frac{\rho_D}{V_D}\left(\frac{\rho_{ref}}{\rho_D}\dot{Q}_{ED} - \dot{Q}_{DC}\right) \quad \text{for inspiration} \qquad (13A)$$

$$\frac{d\rho_D}{dt} = \frac{\rho_D}{V_D}\left(\dot{Q}_{ED} - \frac{\rho_C}{\rho_D}\dot{Q}_{DC}\right) \quad \text{for expiration} \qquad (14A)$$

In this paper, the variation of the total air density throughout the pulmonary pathways is assumed to be negligible. Hence, the time derivatives of the density terms are set to zero in *Eqs. 8A–14A*, and the ratio of density terms are set to one in *Eqs. 8A–11A* and *14A*. For ease of implementation, the density terms are replaced by the corresponding pressure terms by substituting for the constitutive equation of state (ideal gas law).

Blood side. The pulmonary capillary is modeled as a lumped compliant element the volume of which varies in time and is governed by pleural and alveolar pressure changes. Resistance to blood flow through the pulmonary vasculature is partitioned into *1*) extra-alveolar resistances of the pulmonary arteries and veins modulated by the pleural pressure and *2*) intra-alveolar resistance of the capillaries modulated by the alveolar pressure. The mean pulmonary arterial and venous hydrostatic pressures (Ppa and Ppv) are assumed to be constant and are denoted by constant-pressure sources of 15 and 5 Torr relative to the intrathoracic pleural pressure, respectively. Pulsatile effects resulting from the pumping of the right ventricle and left atrium during the cardiac cycle are hereby ignored. The corresponding dynamic equations are given as

$$\frac{dVpc}{dt} = \frac{(Pa - Ppc)}{Ra + Rpc/2} - \frac{(Ppc - Pv)}{Rv + Rpc/2} \qquad (15A,a)$$

$$Ppc = Ptm_b + P_A \qquad (15A,b)$$

$$Ra = [V_\phi(V_A - V^*)^4 + Ra_0]\left(1 + \frac{\overline{Ppl}}{P_\phi}\right) \qquad (15A,c)$$

$$Rv = [V_\phi(V_A - V^*)^4 + Rv_0]\left(1 + \frac{\overline{Ppl}}{P_\phi}\right) \qquad (15A,d)$$

$$Rpc = Rpc_0\left(\frac{Vpc_{max}}{Vpc}\right)^2 \qquad (15A,e)$$

Ptm_b exhibits qualitative characteristics similar to those described for the collapsible airways and is given by

$$ma \times \frac{Vpc_{max} - 0.001}{Vpc_{max} - 13.6\,\overline{C}pc - 0.001} \qquad (16A,a)$$

$$mb = \frac{13.6}{6.908 + \ln(ma - 0.999)} \qquad (16A,b)$$

$$mc = 20.4 - 6.908mb \qquad (16A,c)$$

$$Ptm_b = mc - mb\ln\left(\frac{Vpc_{max} - 0.001}{Vpc - 0.001} - 0.999\right) \qquad (16A,d)$$

The forms for *Eqs. 15A,c* through *15A,e* were dictated by the observation that the extra-alveolar resistances decrease while the intra-alveolar resistance increases during lung inflation (39). The large excursion in the perivascular intrapleural pressure modulates the extra-alveolar resistances and is described by an empirical expression given in *Eqs. 15A,c* and *15A,d*. The parameters Ra_0, Rv_0, Rpc_0, V_ϕ, Vpc_{max}, $\overline{C}pc$, and P_ϕ are determined through the parameter-estimation scheme.

Gas Exchange

Air side. Each of the airway compartments is assumed to be well mixed (hence, no spatial variation within). A generation term representing gas exchange across the alveolar-capillary barrier is present in the alveolar compartment only; no generation terms are present in the descriptions for the rigid and collapsible airway compartments. Inspiratory and expiratory phases are treated separately in the ventilated airways. Species molar balance equations describing the change in partial pressure of the alveolar gaseous species i can be written for each of the compartments as (adapted and modified from Ref. 17)

Inspiration

$$\frac{dP_{D_i}}{dt} = \frac{1}{V_D}\left[\dot{Q}_{ED}\frac{Pam_i^{sat}\,T_{body}}{T_{am}} - \dot{Q}_{DC}\,P_{D_i}\right] \qquad (17A)$$

$$\frac{dP_{C_i}}{dt} = \frac{1}{V_C}\left[\dot{Q}_{DC}\,P_{D_i} - \dot{Q}_{CA}\,P_{C_i} - P_{C_i}\frac{dV_C}{dt}\right] \qquad (18A)$$

$$\frac{dP_{A_i}}{dt} = \frac{1}{V_A}\left[\dot{Q}_{CA}\,P_{C_i} - P_{A_i}\frac{dV_A}{dt} - \left(\frac{P_S\,T_{body}}{T_S}\right)\sum_{j=1}^{N_{seg}}\frac{D_{L_i}(P_{A_i} - Pb_i^{(j)})\Delta Vpc^{(j)}}{Vpc}\right] \qquad (19A)$$

Expiration

$$\frac{dP_{D_i}}{dt} = \frac{1}{V_D}[\dot{Q}_{ED}\,P_{D_i} - \dot{Q}_{DC}\,P_{C_i}] \qquad (20A)$$

$$\frac{dP_{C_i}}{dt} = \frac{1}{V_C}\left[\dot{Q}_{DC}\,P_{C_i} - \dot{Q}_{CA}\,P_{A_i} - P_{C_i}\frac{dV_C}{dt}\right] \qquad (21A)$$

$$\frac{dP_{A_i}}{dt} = \frac{1}{V_A}\left[\dot{Q}_{CA}\,P_{A_i} - P_{A_i}\frac{dV_A}{dt} - \left(\frac{P_S\,T_{body}}{T_S}\right)\sum_{j=1}^{N_{seg}}\frac{D_{L_i}(P_{A_i} - Pb_i^{(j)})\Delta Vpc^{(j)}}{Vpc}\right] \qquad (22A)$$

Blood side. The lumped pulmonary capillary is spatially discretized into equal compartments ($N_{seg} = 35$), and species molar balance is employed to describe the dynamics of the species concentration in each of the discretized compartments. The corresponding equation for species i in compartment j is given by

$$\frac{\partial Cb_i^{(j)}}{\partial t} = -\frac{\partial(V_{z_b}^{(j)}Cb_i^{(j)})}{\partial z} + \frac{D_{L_i}(P_{A_i} - Pb_i^{(j)})}{Vpc} \qquad (23A)$$

The first-order spatial derivative is approximated by using a four-point upwind biased quadratic interpolation formula (47). Fictitious points created at the capillary entrance and exit are eliminated by using the physical and numerical boundary conditions at the entrance and exit, respectively. The effective diffusing capacities for each species (in units of ml $\text{STPD}\cdot\text{min}^{-1}\cdot\text{mmHg}^{-1}$) are designed to account for changing capillary blood volume by scaling the nominal values (17,

22, 35) as shown under

$$D_{L_{O_2}} = \sqrt{\frac{Vpc}{Vpc_{max}}}\,(23.86 + 0.5119\,P_{O_2} - 0.007983\,P_{O_2}^2 + 2.306 \times 10^{-5}\,P_{O_2}^3) \quad (24A,a)$$

$$D_{L_{CO_2}} = \sqrt{\frac{Vpc}{Vpc_{max}}} \times 400.0 \quad (24A,b)$$

$$D_{L_{N_2}} = \sqrt{\frac{Vpc}{Vpc_{max}}} \times 15.0 \quad (24A,c)$$

APPENDIX B

A nonlinear least squares parameter-identification algorithm [Marquardt-Levenburg (30)] is applied to achieve fits to the flow, lung volume, and expired gas concentrations (P_{O_2} and P_{CO_2}) during an FVC maneuver. The objective function employed is the square of weighted residuals in flow, total lung volume, and expired O_2 and CO_2 concentrations at the mouth and is expressed as $\Omega = (\sqrt{\mathbf{W}}\underline{\mathbf{e}})^{\top}(\sqrt{\mathbf{W}}\underline{\mathbf{e}})$. One may define an alternate concatenated error vector, $\underline{\mathbf{e}}^* = \sqrt{\mathbf{W}}\underline{\mathbf{e}}$, in terms of the weighted residuals as follows

$$\underline{\mathbf{e}}^{*\top} = (\sqrt{\omega_{v1}}e_{v1}, \ldots, \sqrt{\omega_{vm}}e_{vm}, \sqrt{\omega_{f1}}e_{f1}, \ldots, \sqrt{\omega_{fm}}e_{fm}, \sqrt{\omega_{O_2 1}}e_{O_2 1}, \ldots, \sqrt{\omega_{O_2 m}}e_{O_2 m}, \sqrt{\omega_{CO_2 1}}e_{CO_2 1}, \ldots, \sqrt{\omega_{CO_2 m}}e_{CO_2 m}) \quad (1B)$$

In *Eq. 1B*, the elements of the positive definite diagonal matrix $\mathbf{W}$, ω_{rs}, are the individual weights assigned to each residual r at time t_s (r = flow at the mouth, total lung volume, expired P_{CO_2}, and expired P_{O_2}). The individual weights are determined by imposing penalty functions (16) associated with specific portions of the time record, as discussed below. The estimation problem now translates to the determination of the elements of the parameter vector $\boldsymbol{\alpha}$ that minimizes a scalar functional $\Omega = \underline{\mathbf{e}}^{*\top}\underline{\mathbf{e}}^*$. This is accomplished by using the Levenburg-Marquardt procedure with the modified error term $\underline{\mathbf{e}}^*$.

In the first stage of adjustment, and during the inspiratory phase with full muscular effort, the parameters that describe the compliant and resistive properties of the alveolar space (ξ, V*), small airways (Rs_m, Rs_a), collapsible airways (inspiratory K_3, Vc_{max}, Ptm_{max}), and upper airways (K_2 for inspiration) were estimated (refer to APPENDIX A). In the following expiratory phase, the estimation method was used to determine other parameters related to the small airways (Rs_a, Rs_m, V_{crit}, Rs_{cmax}), collapsible airways (expiratory K_3), and upper airways (K_2 for expiration). The combined parameter estimate then provided a good fit to both the inspiratory and expiratory portions of the flow-volume loop. In the second stage of adjustment, previously identified parameters were now held unchanged, and the estimation procedure was invoked (for both inspiratory and expiratory phases) to estimate the parameters describing the pulmonary circulation and gas exchange (Ra_0, Rv_0, Rpc_0, V_ϕ, Vpc_{max}, $\overline{C}pc$, and P_ϕ). At this time, the expired P_{O_2} and P_{CO_2} values at the mouth were utilized as the data for the estimation algorithm.

Assignment of Weights

Certain regions of the flow-volume loop are emphasized in identifying the model parameters: *1*) total lung volume; *2*) peak inspiratory flow; *3*) peak expiratory flow; and *4*) the slope of the flow-volume relationship (effort independent) at low lung volumes near RV. A penalty function is imposed by increasing the weighting elements ω_{rs} in these regions to indicate their importance in achieving good fits to the data. These regions are believed to have clinical significance in diagnosis of pulmonary mechanics abnormalities. Initial values of ω_{rs} are uniformly set as $\omega_{vs} = 1$, $\omega_{fs} = 5$, $\omega_{O_{2s}} = 1$ and $\omega_{CO_{2s}} = 1$. The penalty functions imposed at specific time points modify the weighting factors at those points and are as described below.

1. TLC fit. This is enforced only during the inspiratory phase. For the data points in the volume range TLC − 0.5 liters ≤ ($V_A + V_C + V_D$) ≤ TLC, a penalty is enforced on e_{vs} in *Eq. 1B* and the weighting factor is given as $\omega_{vs} = 1 + (100 \times |TLC^{model} - TLC^{data}|)$.

2. Peak inspiratory flow fit. The weighting factor for the inspiratory flow is given as $\omega_{fs} = 1 + (1{,}000 \times |\text{peak } \dot{V}A_o^{model} - \text{peak } \dot{V}A_o^{data}|)$. This is used only for those time points when flow at the mouth is within 0.5 l/s of the peak $\dot{V}A_o$ data values (mid one-thirdof VC).

3. Peak expiratory flow fit. During expiration, $\omega_{vs} = 1 + (1{,}000 \times |\text{peak } \dot{V}A_o^{model} - \text{peak } \dot{V}A_o^{data}|)$ and $\omega_{fs} = 5 + (1{,}000 \times |\text{peak } \dot{V}A_o^{model} - \text{peak } \dot{V}A_o^{data}|)$ for those time points when the flow at the mouth is within 1 l/s below the peak $\dot{V}A_o^{data}$ (highest two-third of VC). The data sampling in the vicinity of the expiratory peak is very sparse, thus requiring a larger weighting factor compared with the other weights.

4. Expired CO_2 and O_2 at the mouth fit. Penalty is imposed to achieve good fits on the phase III plateau of the profile of CO_2 and O_2 concentration in the expirate. The weighting factors are given as $\omega_{CO_2} = 100.0$, $\omega_{O_2} = 10.0$.

Penalty and barrier functions constitute a global approach to nonlinear programming in which weighting factors are incorporated into objective functionals to enforce a specific search direction, thereby accelerating rate of convergence.

The support and encouragement of Dr. L. C. Sheppard is highly appreciated. The authors also thank Dr. S. T. Kuna, Pulmonary Division, Dept. of Internal Medicine at the University of Texas Medical Branch, Galveston, TX, for the use of his laboratory facilities and Dr. F. Ghorbel and Athanasios Athanasiades, Dept. of Mechanical Engineering, Rice University, Houston, TX, for assistance and useful discussions.

Financial support for this work, provided by the Biomedical Engineering Center at the University of Texas Medical Branch, Galveston, TX, is gratefully acknowledged. Additional financial support, provided to A. Bidani by the Moody Foundation, Galveston, TX (no. 94-48) and to J. B. Zwischenberger and A. Bidani by The Shriner Hospital for Crippled Children, Galveston, TX (no. 15859) is also deeply appreciated.

Address for reprint requests: J. W. Clark, Jr., Dept. of Electrical and Computer Engineering, Rice University, Houston, TX 77251.

Received 16 June 1997; accepted in final form 5 December 1997.

REFERENCES

1. **Bachofen, H.** Lung tissue resistance and pulmonary hysteresis. *J. Appl. Physiol.* 24: 296–301, 1968.
2. **Barbini, P., G. Cevenini, K. R. Lutchen, and M. Ursino.** Estimating respiratory mechanical parameters of ventilated patients: a critical study in the routine intensive-care unit. *Med. Biol. Eng. Comput.* 32: 153–160, 1994.
3. **Bidani, A., R. W. Flummerfelt, and E. D. Crandall.** Analysis of the effects of pulsatile capillary blood flow and volume on gas exchange. *Respir. Physiol.* 35: 27–42, 1978.
4. **Bouhuys, A.** *Breathing, Physiology, Environment and Lung Disease.* New York: Grune and Stratton, 1974.
5. **Byrne, G. D., and A. C. Hindmarsh.** A polyalgorithm for the numerical solution of ordinary differential equations. *ACM Trans. Math. Software* 1: 71–96, 1975.

6. **Comroe, J. H.** *Physiology of Respiration*. Chicago, IL: Year Book Medical, 1966.
7. **Conrad, S. A., G. T. Kinasewitz, and R. B. George.** *Pulmonary Function Testing—Principles and Practice.* New York: Churchill-Livingstone, 1984.
8. **Cope, D. K., F. Grimbert, J. M. Downey, and A. E. Taylor.** Pulmonary capillary pressure: a review. *Crit. Care Med.* 20: 1043–1056, 1992.
9. **Dawson, C. A., D. A. Rickaby, and J. H. Linehan.** Distributions of vascular volume and compliance in the lung. *J. Appl. Physiol.* 64: 266–273, 1988.
10. **Dawson, S. V., and E. A. Elliott.** Wave-speed limitation on expiratory flow—a unifying concept. *J. Appl. Physiol.* 43: 498–515, 1977.
11. **Dorbin, H. L., K. R. Lutchen, and A. C. Jackson.** Human respiratory input impedance from 4 to 200 Hz: physiological and modeling considerations. *J. Appl. Physiol.* 64: 823–831, 1988.
12. **Douglas, A. R., N. L. Jones, and J. W. Reed.** Calculation of whole blood CO_2 content. *J. Appl. Physiol.* 65: 473–477, 1988.
13. **Elad, D., and S. Einav.** Simulation of airway closure during forced vital capacity. *Annal. Biomed. Eng.* 17: 617–631, 1989.
14. **Elad, D., and R. D. Kamm.** Parametric evaluation of forced expiration using a numerical model. *Trans. ASME* 111: 192–199, 1989.
15. **Fishman, A. P.** Dynamics of the pulmonary circulation. In: *Handbook of Physiology. Circulation*. Washington, DC: Am. Physiol. Soc., 1963, sect. 2, vol. II, chapt. 48, p. 1667–1743.
16. **Fletcher, R.** *Practical Methods of Optimization*. New York: Wiley, 1987.
17. **Flummerfelt, R. W., and E. D. Crandall.** An analysis of external respiration in man. *Math. Bios.* 3: 205–230, 1968.
18. **Fredberg, J. J., and D. Stamenovic.** On the imperfect elasticity of lung tissue. *J. Appl. Physiol.* 67: 2408–2419, 1989.
19. **Friedland, B.** *Control System Design—An Introduction to State-Space Methods.* New York: McGraw-Hill, 1986.
20. **Golden, J. F., J. W. Clark, and P. M. Stevens.** Mathematical modeling of pulmonary airway dynamics. *IEEE Trans. Biomed. Eng.* 20: 397–404, 1973.
21. **Hawkim, T. S., R. P. Michel, and H. K. Chang.** Effect of the inflation on pulmonary vascular resistance by arterial and venous occlusion. *J. Appl. Physiol.* 53: 1110–1115, 1982.
22. **Hlastala, M. P.** A model of fluctuating alveolar gas exchange during the respiratory cycle. *Respir. Physiol.* 15: 214–232, 1972.
23. **Jackson, A. C., and H. T. Milhorn.** Digital computer simulation of respiratory mechanics. *Comput. Biomed. Res.* 6: 27–56, 1973.
24. **Jonson, B., L. Beydon, K. Brauer, C. Mansson, S. Valind, and H. Grytzell.** Mechanics of respiratory system in healthy anesthetized humans with emphasis on viscoelastic properties. *J. Appl. Physiol.* 75: 132–140, 1993.
25. **Lambert, R. K., T. A. Wilson, R. E. Hyatt, and J. R. Rodarte.** A computational model for expiratory flow. *J. Appl. Physiol.* 52: 44–56, 1982.
26. **Li, C. W., and H. D. Cheng.** A nonlinear fluid model for pulmonary blood circulation. *J. Biomech.* 26: 653–664, 1993.
27. **Lin, K. H., and G. Cumming.** A model of time-varying gas exchange in the human lung during a respirtory cycle at rest. *Respir. Physiol.* 17: 93–112, 1973.
28. **Loeppky, J. A., E. R. Fletcher, R. C. Roach, and U. C. Luft.** Relationship between whole blood base excess and CO_2 content in vivo. *Respir. Physiol.* 94: 109–120, 1993.
29. **Lutchen, K. R., F. P. Primiano, and G. M. Saidel.** A nonlinear model combining pulmonary mechanics and gas concentration dynamics. *IEEE Trans. Biomed. Eng.* 29: 629–641, 1982.
30. **Marquardt, D. W.** An algorithm for least-squares estimation of nonlinear parameters. *J. Soc. Industr. Appl. Math.* 11: 431–441, 1963.
31. **Mead, J.** Mechanical properties of lungs. *Physiol. Rev.* 41: 1840–1848, 1961.
32. **Mead, J.** Analysis of the configuration of maximum expiratory flow-volume curves. *J. Appl. Physiol.* 44: 156–165, 1978.
33. **Mead, J., J. M. Turner, P. T. Machlem, and J. B. Little.** Significance of the relationship between lung recoil and maximum expiratory flow. *J. Appl. Physiol.* 22: 95–108, 1967.
34. **Melo, M. F. V., J. A. Loeppky, A. Caprihan, and U. C. Luft.** Alveolar ventilation to perfusion heterogeneity and diffusion impairment in a mathematical model of gas exchange. *Comput. Biomed. Res.* 26: 103–120, 1993.
35. **Milhorn, H. T., and P. E. Pulley.** A theoretical study of pulmonary capillary gas exchange and venous admixture. *Biophys. J.* 8: 337–357, 1968.
36. **Milic-Emili, J., J. Mead, J. M. Turner, and E. M. Glauser.** Improved technique for estimating pleural pressure from esophageal balloons. *J. Appl. Physiol.* 19: 207–211, 1964.
37. **Milnor, W. R.** Pulmonary hemodynamics. In: *Cardiovascular Fluid Dynamics,* edited by D. H. Bergel. New York: Academic, 1972, vol. 2, p. 299–340.
38. **Morris, A. H., R. E. Kanner, R. O. Crapo, and R. M. Garner.** *Clinical Pulmonary Function Testing—A Manual of Uniform Laboratory Procedures.* Salt Lake City, UT: Intermountain Thoracic Soc., 1984.
39. **Nunn, J. F.** *Nunn's Applied Respiratory Physiology* (4th ed.) Boston, MA: Butterworth Heinemann, 1993.
40. **Olender, M. F., J. W. Clark, and P. M. Stevens.** Analog computer simulations of maximum expiratory flow limitation. *IEEE Trans. Biomed. Eng.* 6: 445–452, 1976.
41. **Oppenheim, A. V., and R. W. Schafer.** *Discrete-Time Signal Processing.* Englewood Cliffs, NJ: Prentice Hall, 1989.
42. **Otis, D. R., M. Johnson, T. J. Pedley, and R. D. Kamm.** Role of pulmonary surfactant in airway closure: a computational study. *J. Appl. Physiol.* 75: 1323–1333, 1993.
43. **Popel, A. S.** Analysis of capillary-tissue diffusion in multicapillary systems. *Math. Bios.* 39: 187–211, 1978.
44. **Rohrer, F.** Der strömungswiderstand in den menschlichen atemwegen und der einfluss der unregelmässigen verzweigung des bronchialsystems auf den atmungsverlauf in verschiedenen lungenbezirken. *Pflügers Arch. Gesamte Physiol. Menschen Tiere* 162: 225–299, 1915.
45. **Saidel, G. M., and J. S. Lin.** Transport abnormalities from single breath dynamics of Ar, CO_2 and O_2. *Respir. Physiol.* 64: 253–266, 1986.
46. **Scherer, P. W., S. Gobran, S. J. Aukburg, J. E. Baumgardner, R. Bartkowski, and G. R. Neufeld.** Numerical and experimental study of steady-state CO_2 and inert gas washout. *J. Appl. Physiol.* 64: 1022–1029, 1988.
47. **Schiesser, W. E.** *Computational Mathematics in Engineering and Applied Science, ODEs, DAEs, and PDEs.* Boca Raton, FL: CRC Press, 1994.
48. **Severinghaus, J. W.** Simple, accurate equations for human blood O_2 dissociation computations. *J. Appl. Physiol.* 46: 599–602, 1979.
49. **Stamenovic, D., K. R. Lutchen, and G. M. Barnas.** Alternative model of respiratory tissue viscoplasticity. *J. Appl. Physiol.* 75: 1062–1069, 1993.
50. **Suki, B.** Nonlinear phenomena in respiratory mechanical measurements. *J. Appl. Physiol.* 74: 2574–2584, 1993.
51. **Suki, B., A.-L. Barabasi, and K. R. Lutchen.** Lung tissue viscoelasticity: a mathematical framework and its molecular basis. *J. Appl. Physiol.* 76: 2749–2759, 1994.
52. **Suki, B., and J. H. T. Bates.** A nonlinear viscoelastic model of lung tissue mechanics. *J. Appl. Physiol.* 71: 826–833, 1991.
53. **Thiriet, M., M. Bonis, A. S. Adedjouma, C. Hatzfeld, and J. P. Yvon.** Experimental and theoretical models of flow during forced expiration: pressure and pressure history dependence of flow rate. *Med. Biol. Eng. Comput.* 25: 551–559, 1987.
54. **Tomlinson, S. P., D. G. Tilley, and C. R. Burrows.** Computer simulation of the human breathing process. *IEEE Eng. Med. Biol. Mag.* 13: 115–124, 1994.
55. **Verbraak, A. F. M., J. M. Bogaard, J. Beneken, E. Hoorn, and A. Versprille.** Serial lung model for simulation and parameter estimation in body plethysmography. *Med. Biol. Eng. Comput.* 29: 309–317, 1991.
56. **Wada, S., Y. Seguchi, and M. Tanaka.** Breathing-ventilation model, and simulation of high-frequency ventilation. *JSME Intern. J. Ser. 1* 34: 98–105, 1991.
57. **Weibel, E. R.** *Morphometry of the Human Lung.* Berlin: Springer-Verlag, 1963.
58. **West, J.** *Best's and Taylor's Physiological Basis of Medical Practice.* Baltimore, MD: Williams & Wilkins, 1985.
59. **West, J. B.** *Ventilation/Blood Flow and Gas Exchange* (5th ed.) London: Blackwell, 1990.